Analysis of ice temperatures of four selected very small glaciers in the Swiss Alps by means of modelling and ground penetrating radar

GEO 511 Master Thesis in Physical Geography

Department of Geography, University of Zurich

Nadia Signer

08-917-536

September 2014

Supervisors:

Dr. Matthias Huss
ETH Zürich
HIT F43
Wolfgang-Pauli-Strasse 24
8093 Zürich
huss@vaw.baug.ethz

MSc Mauro Fischer
University of Fribourg
Office 336
Chemin du Musée 4
1700 Fribourg
mauro.fischer@unifr.ch

Faculty Member:

Prof. Dr. Andreas Vieli

Nadia Signer

Dörflistrasse 44

8050 Zürich

nadia.signer@hotmail.com

Preface

I have always been fascinated by snow and ice, especially by high mountain areas with their amazing glaciers. Since my early Bachelor studies I focussed on the abiotical part of physical geography. During my Master studies, I deepened my interest in processes of high-mountain areas in the minor subject of glaciology. The present thesis has given me the opportunity to get even deeper in the matter. I chose the topic of very small glaciers because until now not much knowledge exists about them and I hope to contribute a little piece to the further understanding of very small glaciers.

During my thesis, I could gain experience in many different fields, which made the work very diversified. At the beginning of my thesis, I could assist to install thermistor chains at Glacier du Sex Rouge. The fieldwork was very interesting, not only because of the beautiful sunrise over the breath-taking panorama. Back home, I was introduced to the analysis of radar profiles as well as the modelling with GERM. The detailed confrontation with the model helped to better comprehend modelling approaches in general.

At this point I want to express my sincere thanks to everyone who contributed to the completion of my thesis. First of all I want to thank my supervisors Matthias Huss and Mauro Fischer: Matthias for answering my countless questions and emails and never losing patience with my technical modelling problems, and Mauro for supplying me with measurement data, for always having an open ear for my problems and for encouraging me with his positive attitude. Further thanks go to thank Andreas Vieli for his comments on my concept. Furthermore I want to thank Patrick Hager for providing me his ice measurement data from Vadret dal Corvatsch and for his interest in my work.

Special thanks go to my parents Marie-Claire and Ernst Signer for their continuous support and their encouragement during all my studies, to my sisters Daniela and Lilian for distracting me and bringing me back down to earth, and to Tobi for his comfort. Last but not least I want to thank my fellow students for inspiring discussions and the motivating coffee breaks.

Abstract

Although very small glaciers (< 0.5 km^2) represent *in number* the biggest size class in the Swiss Alps, not much knowledge exists about them. In order to further understand important prevailing processes of very small glaciers, ice temperatures of Vadret dal Corvatsch (GR), Glacier du Sex Rouge (VD), St. Annafirn (UR) and Pizolgletscher (SG) were examined using different techniques. Englacial temperatures were modelled using an adapted version of the Glacier Evolution Runoff Model (GERM). Furthermore, the thermal regime was investigated using ground penetrating radar. The obtained data was then compared to measured borehole temperatures.

First borehole measurements show, that cold ice can also be found at very small glaciers, even though they are situated at elevation where cold ice wouldn't be expected. It can be assumed that the presence of cold ice at very small glaciers is closely linked to glacier hydrology. On one hand, the absence of crevasses due to very low movement prevents water to penetrate the glacier. On the other hand, very small glaciers experience extended melting of firn – allowing the winter cold to enter the glacier easily and withdrawing the possibility to store meltwater at the glacier surface. Thus, meltwater exits the glacier supraglacially and no major refreezing occurs at the glacier surface. (Gilbert *et al.* 2012)

Modelling of ice temperatures partially show some major offset of ±1°C to the measured borehole temperatures. Ice temperatures at different locations at the same glacier were modelled too similar. However differences of ice temperatures at different glaciers were represented reasonable. Modelling of ice temperatures over time suggest that temperatures at a depth of 20 m – where seasonal temperature fluctuations vanish– experienced a decrease up to the early 21st century. Since 2005-2010 modelled 20m-temperatures are increasing until the complete disappearance of the glaciers.

The analysis of radar profiles revealed the depth of a water-saturated layer present at certain areas of the glaciers. Its comparison to the cold-transition surface (CTS) showed that differences lay within the range of uncertainty. However such a comparison was only possible for one borehole at Glacier du Sex Rouge and further measurements are required to consolidate this agreement.

Contents

List of Figures

List of Tables

List of Abbreviations

CTS	Cold-temperate transition surface
ELA	Equilibrium line altitude
DEM	Digital elevation model
GERM	Glacier Evolution Runoff Model
GIS	Geographic information system
GPR	Ground penetrating radar
GPS	Global Positioning System
MAAT	Mean annual air temperature
MAFT	Mean annual firn temperature
PMP	Pressure melting point
RADAR	Radio detecting and ranging
RMSE	Root mean square error
RTS	Radar transition surface

Abbreviations for individual glaciers

COR	Vadret dal Corvatsch
PZL	Pizolgletscher
SER	Glacier du Sex Rouge
STA	St. Annafirn

1. Introduction and scientific background

Glaciers worldwide continue to shrink and the Northern Hemisphere spring snow cover continues to decrease in extent (IPCC 2013). This development is also recorded in the Swiss Alps and will have major impacts on the high-mountain hydrology (e.g. Viviroli *et al.* 2011, Bavay *et al.* 2013) and on mass-movement processes (e.g. Stoffel and Huggel 2012). Until today, the contribution of medium and large (valley) glaciers to these changes has been examined in several studies (e.g. Oerlemans *et al.* 2009, Huss *et al.* 2010c, Farinotti *et al.* 2012). At the same time not many glaciological measurements have been carried out on very small glaciers (<0.5 km^2). Therefore, there is considerable uncertainty in modelling their mass balance response to the ongoing climate change (Kuhn 1995, Huss 2010). Furthermore, only few is known about the dynamics and thermal regime of very small glaciers, which makes it difficult to predict the future lifetime and the assessment of the impact of the likely disappearance of very small glaciers throughout the next decades. In view of the challenges of the changing climate, it is however important to understand all components of the cryosphere, particularly since very small glaciers are numerous in most glacierized areas around the world (Bahr and Radić 2012). If cold ice exists at very small glaciers, the potential use of the glacier ice as palaeo-climatic ice archives is basically possible (Haeberli *et al.* 2004).

1.1. Characteristics of very small glaciers

Very small glaciers represent, in number, the largest size class in the European Alps. According to the new Swiss Glacier Inventory SGI2010 compiled by Fischer *et al.* (2014a), 82.1% of the *number*s of glaciers are classified as very small glaciers. In return, their *total area* only covers 12.5% of the entire glacierized area in Switzerland (Table 1.1).

Table 1.1: Numbers and surface areas of very small glaciers in the Swiss Alps. Selected numbers from the new Swiss Glacier Inventory SGI2010 compiled by Fischer *et al.* (2014a)

		Number of glaciers		Surface area	
1973	Very small glaciers (0 - 0.5 km^2)	1773	82.3 %	204.4 km^2	15.6 %
	All size classes	2155	100 %	1306.9 km^2	100 %
2010	Very small glaciers (0 - 0.5 km^2)	1165	82.1 %	118.0 km^2	12.5 %
	All size classes	1419	100 %	944.1 km^2	100 %

1.1.1. Mass balance

Very small glaciers show both high accumulation and ablation rates (Kuhn 1995). Several studies have shown that very small glaciers can be found where enhanced accumulation by avalanching and wind drift as well as reduced ablation by shading occurs (e.g. Kuhn 1995, Chuece *et al.* 2007, Huss 2010, Bahr and Radić 2012). Due to these topoclimatic conditions, very small glaciers are present far below the regional climatic equilibrium line altitude (ELA). For example in the Mediterranean area, where the regional ELA is located over 3000 m a.s.l., the Debeli Namet glacier in Montenegro at 2050-2300 m a.s.l. (Hughes 2007, 2008) and the Ghiacciaio del Calderone in Italy at 2760 - 2839 m a.s.l (Gellatly *et al.* 1994) still exist. In Switzerland, almost half of the very small glaciers (556 of 1165, 47.7%) don't reach 3000 m a.s.l. (Fischer *et al.* 2014a), whereas the mean climatic ELA is situated at around 3000 m a.s.l in the European Alps (Zemp *et al.* 2007).

1.1.2. Surface area changes

For the observation period 1973-2010, Fischer *et al.* (2014a) show that – in contrast to larger glaciers – relative area changes of very small glaciers varied over a large range (Figure 1.1). The decreasing mean of relative area changes towards smaller glaciers points to the importance not to neglect small glaciers in inventories, as significant errors in the assessment of regional glacier change may occur.

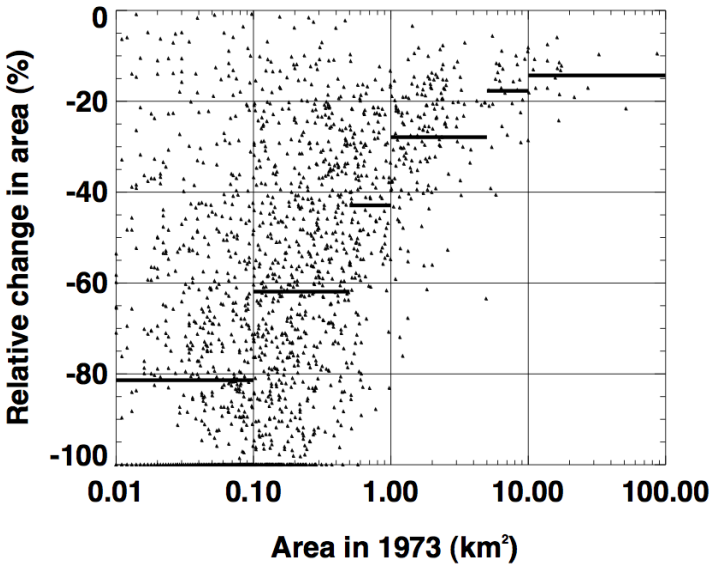

Figure 1.1: Observed relative changes in surface area 1973–2010 versus initial surface area. Horizontal lines show average values for individual size classes (in km²: <0.1, 0.1–0.5, 0.5–1.0, 1.0–5.0, 5.0–10.0, >10.0). (Fischer *et al.* 2014a)

While relative changes in area were highest for very small glaciers, the percentaged size-class distribution hardly changed between 1973 and 2010 (Table 1.1). It has to be noted that changes of number and area might also be a result of shifts in size classes (Fischer *et al.* 2014a).

On a shorter timescale, very small glaciers may reveal positive surface area changes. In years with high accumulation by wind-drift and avalanches, very small glaciers can possibly grow substantially. However, this length gains can be lost equally fast during warm years because the frontal glacier section only consisted of a shallow multi-year firn field connected to the main ice body. The effect of this process possibly leads to irregular glacier margins. (Huss 2010)

1.1.3. Sensitivity to climate change

López-Moreno *et al.* (2006) showed that during the final stages of a glacial degradation process, the relative influence of climatic factors linked to altitude – such as temperature, precipitation and the ratio in precipitation of snow to rain – decreases. At the same time, the influence of topographic-induced conditions – as the exposure to solar radiation and the terrain curvature – increases. Glaciers might even become insensitive to regional climatic changes due local topoclimatic factors favouring avalanching and shading (Hughes 2009). Therefore, it is questionable whether very small glaciers are reliable indicators of climate change (e.g. DeBeer and Sharp 2009). However, very small glaciers may disappear or reform within a few years because of their fast response in temperature and precipitation changes (Kuhn 1995). Yet, the vast majority of very small glaciers show negative mass balance values over several years and it is very likely that most of them will vanish within the next decades (e.g. Zemp *et al.* 2006, Huss 2012).

1.1.4. Ice temperatures

Until today only very few measurements of englacial temperatures have been carried out on small glaciers. To our knowledge, ice temperatures of only one very small glacier in Switzerland were measured; borehole temperatures were carried out at Vadret dal Corvatsch in view of the potential use of the ice crest as palaeo-climatic archive (Hager 2002, Haeberli *et al.* 2004). There, cold ice (ice below the pressure melting point, for further explanations see page 6) could be found at the exposed ice crest at an altitude of about

3340 m a.s.l. Temperatures at a depth of 13 m, where the seasonal temperature variability was only minor, were around -4° C between 2000 and 2002. (Hager 2002)

A recent study (Gilbert *et al.* 2012) showed an interesting evolution of ice temperatures of a very small glacier located in the French Alps. Tête Rousse Glacier is situated at an elevation range of 3100-3300 m a.s.l. and has an area of 0.08 km^2 (2007). The glacier was investigated due to its tendency for subglacial lake outbursts and flood hazards. Although the existence of cold ice would not be a big surprise at this elevation, the evolution of the englacial temperature is surprising. Temperature measurements showed a polythermal structure; meaning that both ice below and ice at the pressure melting point are coexisting within the glacier (for further explanations see page 6). Subglacial water is trapped by the impermeable cold lowest part of the glacier. What might be counterintuitive, periods with negative mass balance – associated with higher air temperatures – tend to cool the glacier. In years with lower air temperatures, englacial temperatures tend to increase ice temperatures of Tête Rousse Glacier. Gilbert *et al.* (2012) explain these observations with the abundance of firn. If the firn cover melted as a consequence of higher air temperatures, no meltwater is stored at the glacier surface and it exits the glacier supraglacially. Thus, no warming due to the release of latent heat during refreezing processes occurs.

1.2. Aims and research objectives

As not many studies have been carried out on very small glaciers, and ice temperatures are crucial for the understanding of predominant processes in a glacier, the present thesis focuses on the thermal regime of very small glaciers. Thereby, several aspects of temperature measurements and modelling are examined, and the following research questions were set:

1. Do **very small glaciers** in the Swiss Alps **contain cold ice** although temperate ice would be expected at their altitude?
2. Is it possible to **model ice temperatures** of very small glaciers with an adapted version of the GERM model? Can the model be used to model **future ice temperatures**?
3. Is it possible to detect cold ice within very small glaciers by means of **GPR** data?

To answer these questions, the following strategies were chosen:

1. The thermal regimes of three selected very small glaciers in the Swiss Alps were investigated using **temperature measurements in boreholes**. Vadret dal Corvatsch, Glacier du Sex Rouge and St. Annafirn and were chosen as for these very small glaciers temperature measurements were carried out or are running at the moment in the context of the PhD project "New monitoring techniques for understanding the response of very small glaciers to climate change" of Mauro Fischer (University of Fribourg).

2. Ice temperatures of Vadret dal Corvatsch, Sex Rouge and St. Annafirn were modelled. The model was validated with borehole measurements. Additionally, ice temperatures of Pizolgletscher were modelled, for which no temperature measurements were available for comparison.

3. GPR data of Vadret dal Corvatsch, Glacier du Sex Rouge, St. Annafirn and Pizolgletscher were analysed with a special focus on the cold-temperate transition surface (CTS). On some GPR images, a distinct transition between zones of different backscatter intensity can be identified; henceforth referred to as radar transition surface (RTS). These transition horizons are compared with temperature measurements and modelled temperatures to see if it is possible to detect the CTS using GPR data.

1.3. Scientific background

Glaciers of all sizes can be classified according to their englacial temperatures. **Cold** glaciers are defined as firn- and ice bodies showing temperatures below the pressure melting point (PMP) throughout (except for maybe a thin surface layer) and over a minimum of time period of the year (e.g. Cuffey and Paterson 2010). **Temperate** glaciers contain ice at the PMP, except for seasonal freezing of the surface layer. However, the vast majority of glaciers is **polythermal**, meaning that both cold and temperate ice co-exists within the glacier. In polythermal glaciers, the zones of different temperatures are separated by the cold-temperate transition surface (CTS) (Blatter and Hutter 1991). Different patterns of distribution of temperate ice within an otherwise cold glacier exist. The winter cold entering at the surface may lead to a pattern seen in Figure 1.2a. When melt occurs at the surface, a percolation zone may produce a temperate near-surface layer above an otherwise cold ice mass (Figure 1.2b). The most important type of CTS is a temperate base layer, leading to sliding over the bed (Figure 1.2c). A further possible pattern of thermal regime occurs at the confluence of two glaciers of different temperatures or when low temperatures in high accumulation areas are transmitted below the ELA due to thermal advection (Hutter *et al.* 1988).

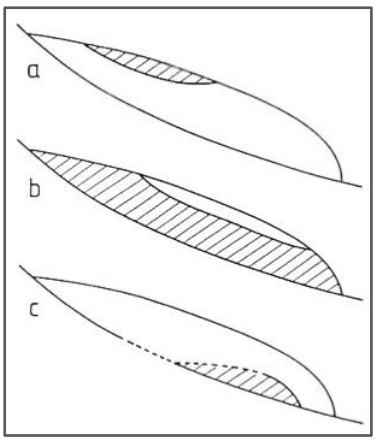

Figure 1.2: Various types of polythermal structures in glaciers. The shaded areas denote temperate parts of the ice and the dashed lines along the cold-temperate transitions indicate parts with melting conditions (modified from Blatter and Hutter 1991).

The thermal regime has strong impacts on the behaviour of glaciers, and can be responsible for differences in ice velocity, erosion and deposition rates, landforms, hydrology and plumbing system, mass balance, and response time. It was shown that cold ice within a polythermal ice body controls its flow dynamics through the temperate dependence of viscosity, and affects glacier hydrology by blocking water flow paths (Ryser *et al.* 2013). Cold-based glaciers – meaning glaciers with a cold bed – are frozen to the ground and

therefore they exhibit lower ice velocities than warm-based glaciers. Thus, cold ice stabilizes glaciers, especially at steep slopes (Goodrich 1982).

Ice temperatures depend on many factors. Heat is transported through a glacier by **heat conduction**, by **thermal advection** through the moving ice, and by **convective heat transfer** through water or air flowing through cracks and channels.

According to Lüthi and Funk (2012), heat sources within the glacier are

- Dissipative heat production due to ice deformation (internal friction)
- Frictional heating at the glacier base (basal motion)
- Frictional heating of flowing water at englacial channel walls
- Release or consumption of latent heat due to freezing and melting

Practically, englacial temperatures are mainly a result of the energy- and mass balance at the glacier surface. Important parameters are mean annual air temperature (MAAT), radiation flux, accumulation and ablation rates, meltwater processes in firn areas and crevasses, topographic location and wind effects (e.g. Suter *et al.* 2001). As air temperatures and accumulation rates are two of the main drivers of firn temperatures, the thermal regime of glaciers can be linked to the MAAT and the amount of precipitation. According to the cryosphere model after Shumsky (1964) and Haeberli (1985) in Figure 1.3, cold ice exists at locations with MAAT below -8°C, whereas cold firn already develops at locations with MAAT below -2°C.

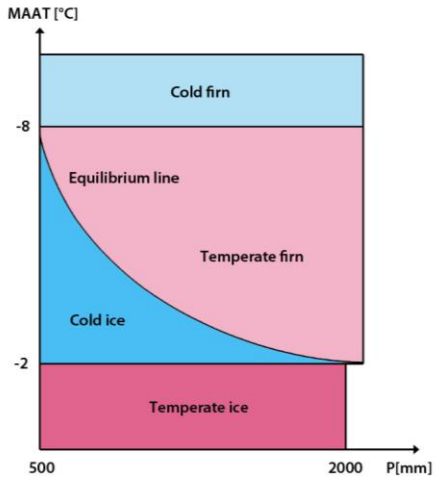

Figure 1.3: The cryosphere model after Shumsky (1964) and Haeberli (1985) shows the thermal regime of glaciers as a function of mean annual air temperatures (MAAT) and the annual precipitation. (Modified from Hoelzle 1994)

Seasonal temperature fluctuations are predominant in the uppermost 10-20 m of the firn body. Temperatures to this depth shall be called near-surface firn temperatures after Hooke *et al.* (1983).

1.4. Cold ice in the Swiss Alps

In the European Alps, glaciers are generally temperate. Still, temperatures at elevation of more than 4000 m a.s.l. are low enough for the existence of cold glacier ice (e.g. Eisen *et al.* 2009, Ryser *et al.* 2013). Haeberli *et al.* (2004) made a compliation of englacial temperatures compared with the according altitude of the drilling sites. According to Figure 1.4 one would not expect cold ice at altitudes below around 3000 m a.s.l.

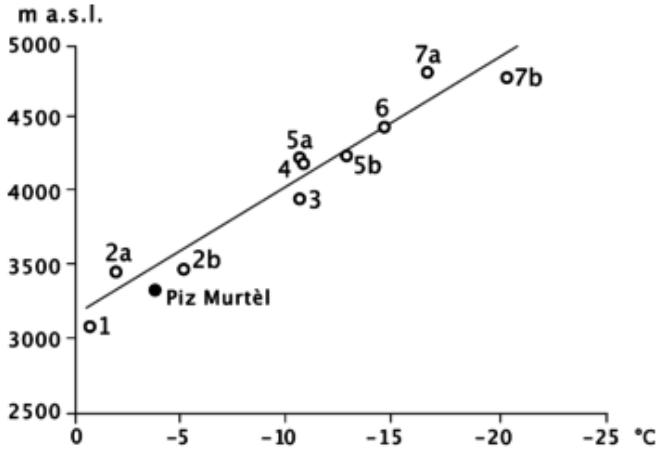

Figure 1.4: Compilation of mean annual temperatures within cold firn and ice in the European Alps from Haeberli *et al.* (2004). 1 Chli Titlis, 2a Jungfraujoch saddle, 2b Jungfraujoch (crest), 3 Fleschhorn, 4 Dufoursattel, 5a/5b Col du Dôme, 6 Colle Gnifetti, 7a/7b Mont Blanc.

Also Suter *et al.* (2001), who took into account that ice temperatures depend on the aspect, propose that cold firn is not possible below 3000; even at north facing slopes (Table 1.2).

Table 1.2: Lower boundaries of possible or probable cold-firn occurrence according to a firn map by Suter *et al.* (2001).

Aspect	Cold firn possible above [m a.s.l.]	Cold firn probable above [m a.s.l.]
N	3000	3400
NE/NW	3000	3600
E/W	3300	3800
SE/SW	3550	3950
S	3700	4150

1.4.1. Cold ice at high altitudes

Cold ice at altitudes of more than 3000 m a.s.l. results from air temperatures below the freezing point throughout the year. If meltwater is produced at the surface, it refreezes within the firn pack, without reaching the glacier ice (Figure 1.5). Ice temperatures remain below the PMP since no latent heat is released within the glacier (Suter and Hoelzle 2002).

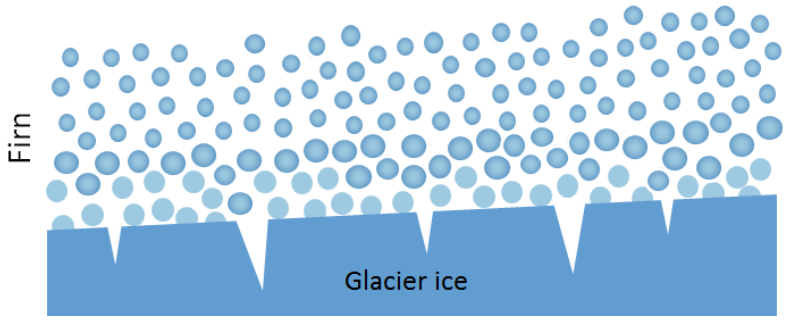

Figure 1.5: If air temperatures are low enough, all produced meltwater at the surface refreezes within the firn pack and is thus unable to reach the glacier ice.

Cold ice at high altitudes builds up in the accumulation zone and then flows downwards, where it eventually exits the glacier below the equilibrium line (Ryser *et al.* 2013). This can be observed, for example, at Grenzgletscher in the canton of Valais (Switzerland). Its accumulation area starts at Seserjoch and Colle Gnifetti (4450 m a.s.l.), while its terminus is located at an altitude of only 2200 m a.s.l. As can be seen in Figure 1.6, temperatures below the PMP could be measured even in the lower ablation area (Ryser *et al.* 2013).

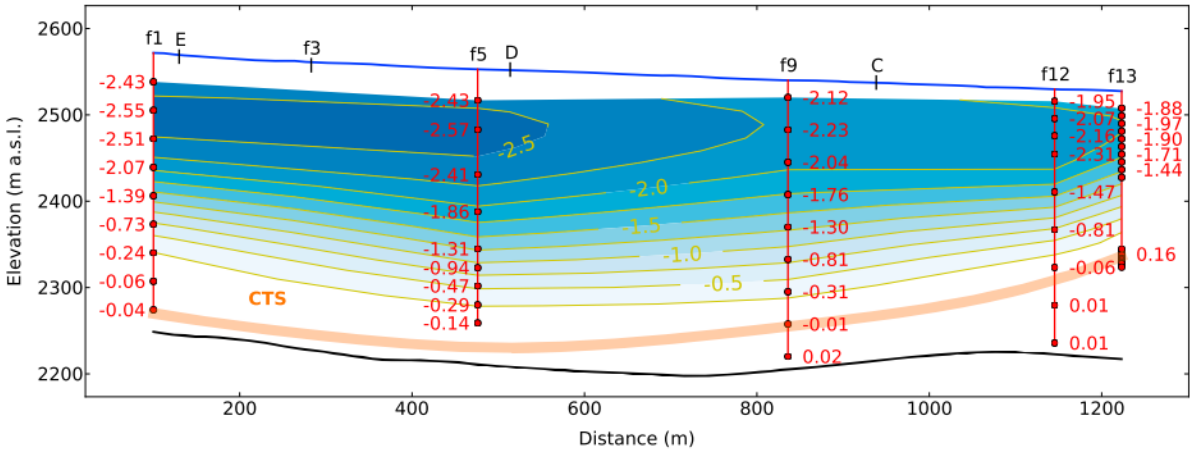

Figure 1.6: Measured and interpolated ice temperatures in the lower ablation area of Grenzgletscher (VS). The vertical red lines show measurements of five boreholes along the central flow line in the lower part of the glacier. The wide orange curve indicates the approximate depth of the CTS. The glacier bed determined from radar is shown in black. The ice is flowing from left to right. (Ryser *et al.* 2013)

1.4.2. Cold ice at very small glaciers

The existence of cold ice in the European Alps is also possible below 3000 m a.s.l., but different conditions lead to the build-up of such. Cold ice develops in ablation areas, where no extended firn areas and no major crevasses are present. The fact that meltwater exits the glacier supraglacially – and is thus unable to warm the glacier – is the driving force of the existence of cold ice (Figure 1.7).

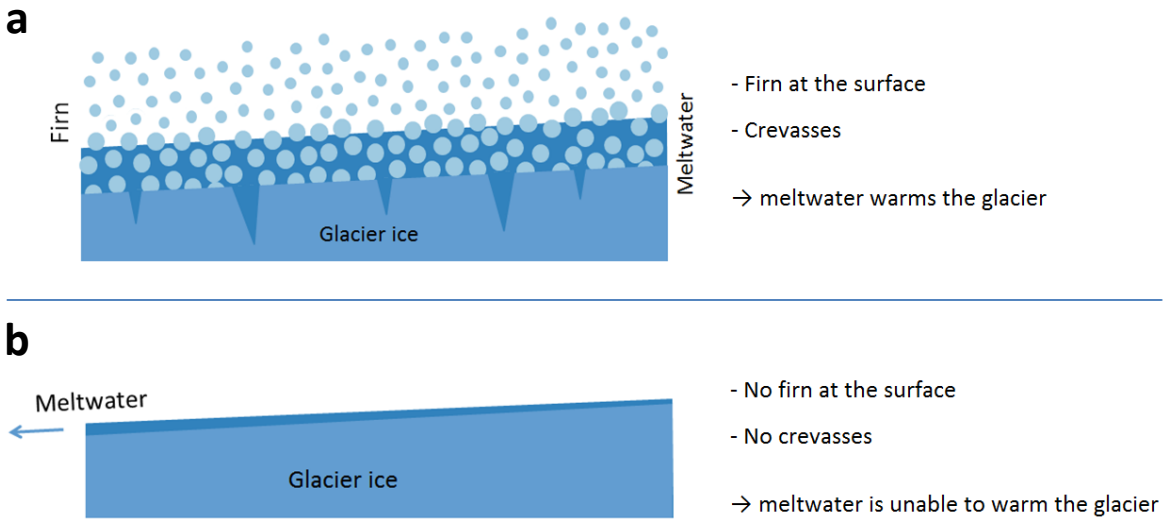

Figure 1.7: Schematic overview of the meltwater situation **(a)** at a glacier with firn and crevasses and **(b)** a glacier without firn and crevasses.

As very small glaciers on rather flat terrain show nearly no movement (Kuhn 1995) no major amount of crevasses opens up due to internal strains within the glacier. Without crevasses, meltwater is not able to penetrate the glacier. Additionally, the absence of extensive firn areas in years with high air temperatures prevents the storage of meltwater at the surface of the glacier, and meltwater exits supraglacially or at the margins. Stored meltwater would lead to a rise of temperature up to the PMP due to refreezing processes within areas of colder firn or ice (Gilbert *et al.* 2012). Furthermore, the lack of an extensive firn area also results in a reduced insulation, letting the winter cold easily enter the glacier ice. At the same time, no enhanced warming takes place in summer, as all incoming energy in form of radiation is used to melt the ice at the surface, which then exits the glacier quickly without causing any warming.

2. Study Sites

Four very small glaciers were chosen for this study. The selected glaciers are well spread over the Swiss Alps at altitudes between 2600-3400 m a.s.l. (Figure 2.1); three of them are situated below 3000 m a.s.l. (Table 3.1). All sites are easy accessible by touristic infrastructure – mainly by cable car – allowing short and efficient field visits. In this section, a short overview of the four glaciers is given. All available datasets are described in detail in the section 3, Datasets.

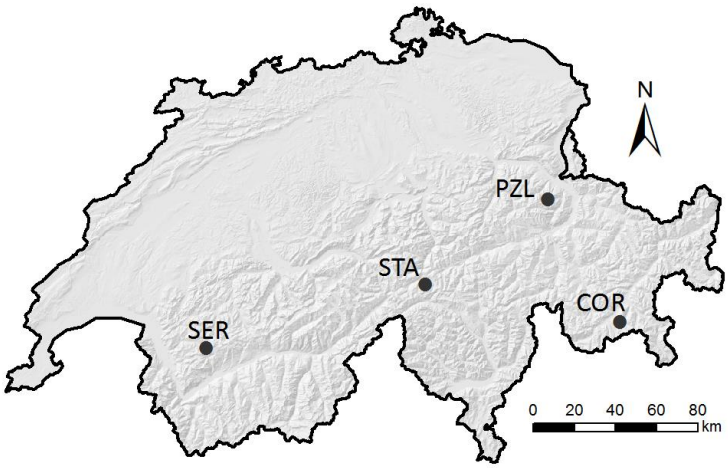

Figure 2.1: Overview of the analysed glaciers. Abbreviations (ordered by area): Vadret dal Corvatsch (COR), Glacier du Sex Rouge (SER), St. Annafirn (STA), Pizolgletscher (PZL).

Table 2.1: Area, location and altitude range of Vadret dal Corvatsch, Glacier du Sex Rouge, St. Annafirn, and Pizolgletscher.

	Area [km^2]	Location	Altitude range [m a.s.l.]
Vadret dal Corvatsch-S (GR)	0.227 (2009)	9.8244°N, 46.4168°E	2934-3417 (2009)
Sex Rouge (VD)	0.270 (2010)	7.2139°N, 46.3274°E	2714-2867 (2010)
St. Annafirn (UR)	0.217 (2010)	8.6027°N, 46.5988°E	2596-2928 (2010)
Pizolgletscher (SG)	0.081 (2010)	9.3912°N, 46.9613°E	2602-2783 (2010)

2.1. Vadret dal Corvatsch

Vadret dal Corvatsch is situated in the centre of the Upper Engadine Valley (GR). Vadret dal Corvatsch has its culmination on Piz Murtèl at an elevation of 3433 m a.s.l. The glacier is divided into two parts, which got disconnected from each other in the last years. In this study, only the southern part of the glacier is investigated. Hereafter the name "Vadret dal Corvatsch" refers only to the southern part of Vadret dal Corvatsch (Vadret dal Corvatsch-S).

Vadret dal Corvatsch has an around 500 m long, slightly asymmetric ice crest at its upper part. The northwest-facing slope is rather steep and approx. 45 m high. When snow-free in summer, annual layers are nicely visible there (Haeberli *et al.* 2004). An ice-dammed lake formed at the foot of the ice crest (Figure 2.2).

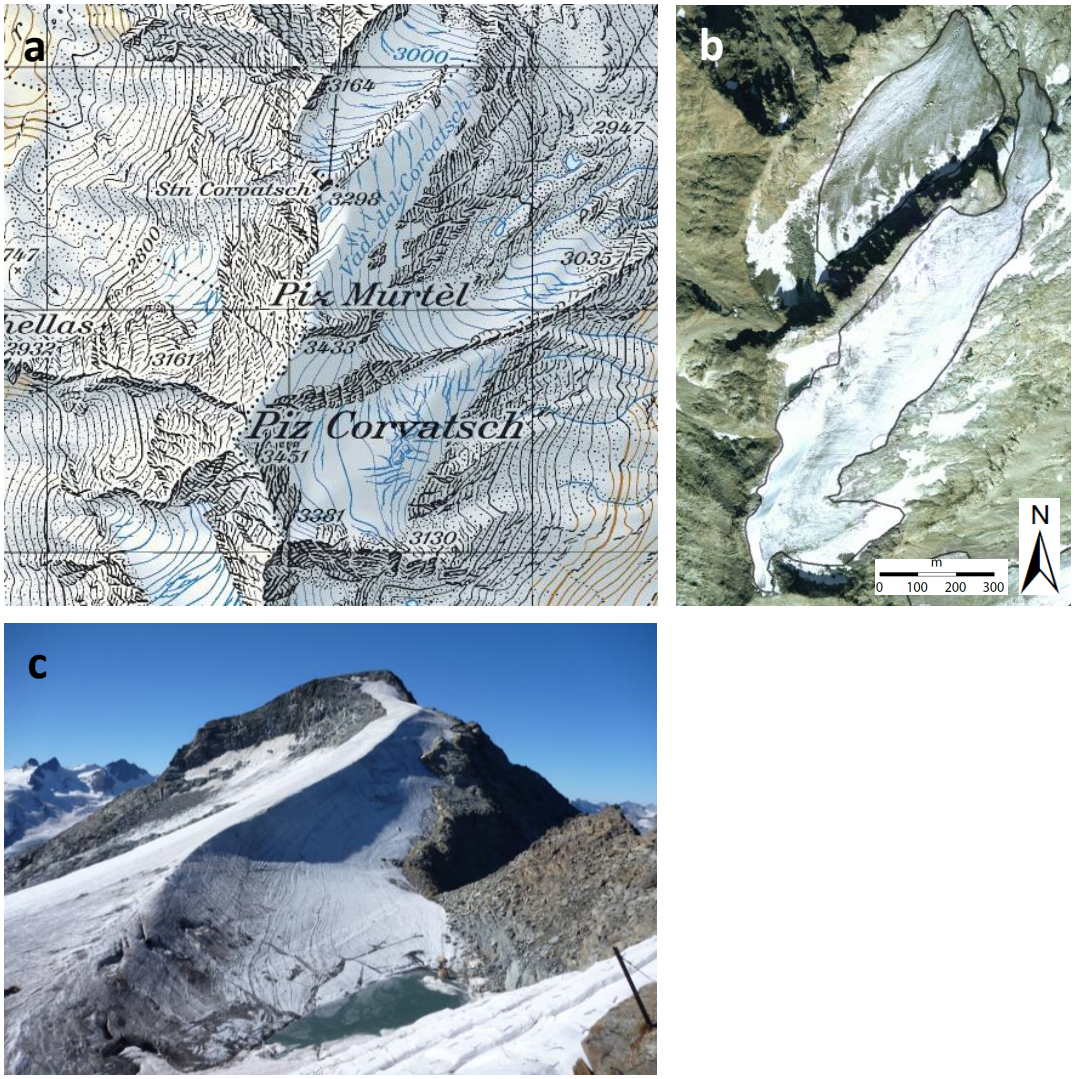

Figure 2.2: **(a)** Vadret dal Corvatsch on the Swiss national map 1:25'000 by the Federal Office of Topography swisstopo. **(b)** Vadret dal Corvatsch on the high-resolution aerial orthophotograph SWISSIMAGE 2012. The outline is taken from the new Swiss Glacier Inventory SGI2010 (Fischer *et al.* 2014a), showing that the two parts are now separated. **(c)** Ice crest of Vadret dal Corvatsch with a little ice-dammed lake near the cable car station. The Picture was taken in August 2012 by Mauro Fischer.

The Upper Engadine is predominantly influenced by weather conditions from the south. Due to protection from clouds by surrounding mountains, the climate is comparatively rather continental; meaning low temperatures in winter and low humidity are prevailing (Hager 2002). A weather station at the upper cable car station right next to the glacier (783155 N 143520 E, 3315 m a.s.l.) is available, providing temperature and precipitation measurements. A climate diagram with mean monthly values for precipitation and air temperatures of the years 1980-2013 is given in Figure 2.3. The mean annual air temperature (MAAT) is -5.2°C and the annual precipitation is 932 mm.

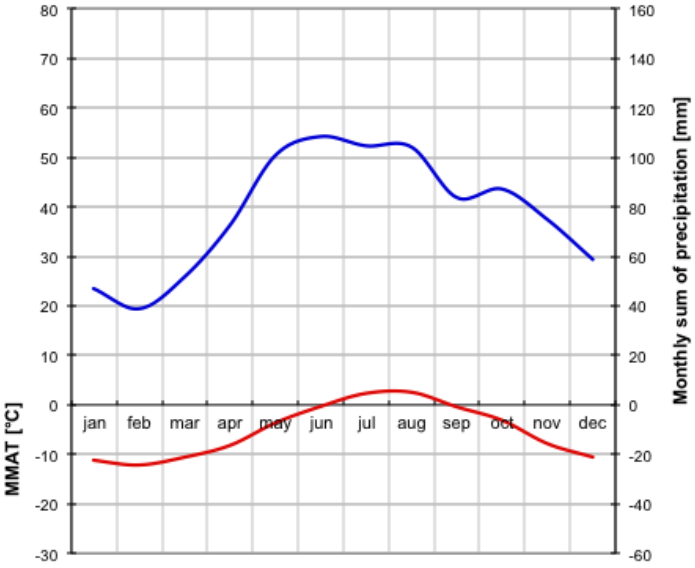

Figure 2.3: Climate diagram with the data of the weather station at the upper cable car station Corvatsch (783155 N/143520 E, 3315 m a.s.l.). Mean monthly air temperature values 2 m above ground (red line, left axis) and sum of monthly precipitation (blue lines, right axis) for the years 1980-2013 are displayed. Data was obtained from the Federal Office of Meteorology and Climatology MeteoSwiss.

According to the cryosphere model (Figure 1.3) and with the described long-term values of air temperature and precipitation, temperate firn but cold ice can be expected for Vadret dal Corvatsch.

The ice crest (Figure 2.2c) at the southern part of the glacier was closely examined in regards of the potential use as a palaeo-climate archive. Therefore, temperature measurements were carried out between 1999 and 2001 at several points at the ice crest (Hager 2002, Haeberli *et al.* 2004). These investigations showed that Vadret dal Corvatsch contains cold ice (see section 0 Datasets). Furthermore several radar profiles were analysed (Busarello 2002). GPR profiles covering the whole glacier were repeated in 2013 by Mauro Fischer.

2.2. Glacier du Sex Rouge

Glacier du Sex Rouge lies west of Oldenhorn, which marks the border between the cantons of Vaud, Bern and Valais. The study site is situated within the ski resort of Glacier 3000 and is therefore easily accessible, even by snow cat. Over the Col de Tsanfleuron, Sex Rouge is connected to the distinctly larger Glacier de Tsanfleuron (Figure 2.4a-b). No major crevasses are present at the glacier as Glacier du Sex Rouge is flowing very slowly – velocities of around 0.5 m were measured from 2012 to 2013 (M. Fischer 2013, personal communication). Glacier du Sex Rouge shows supraglacial drainage channels (Figure 2.4c).

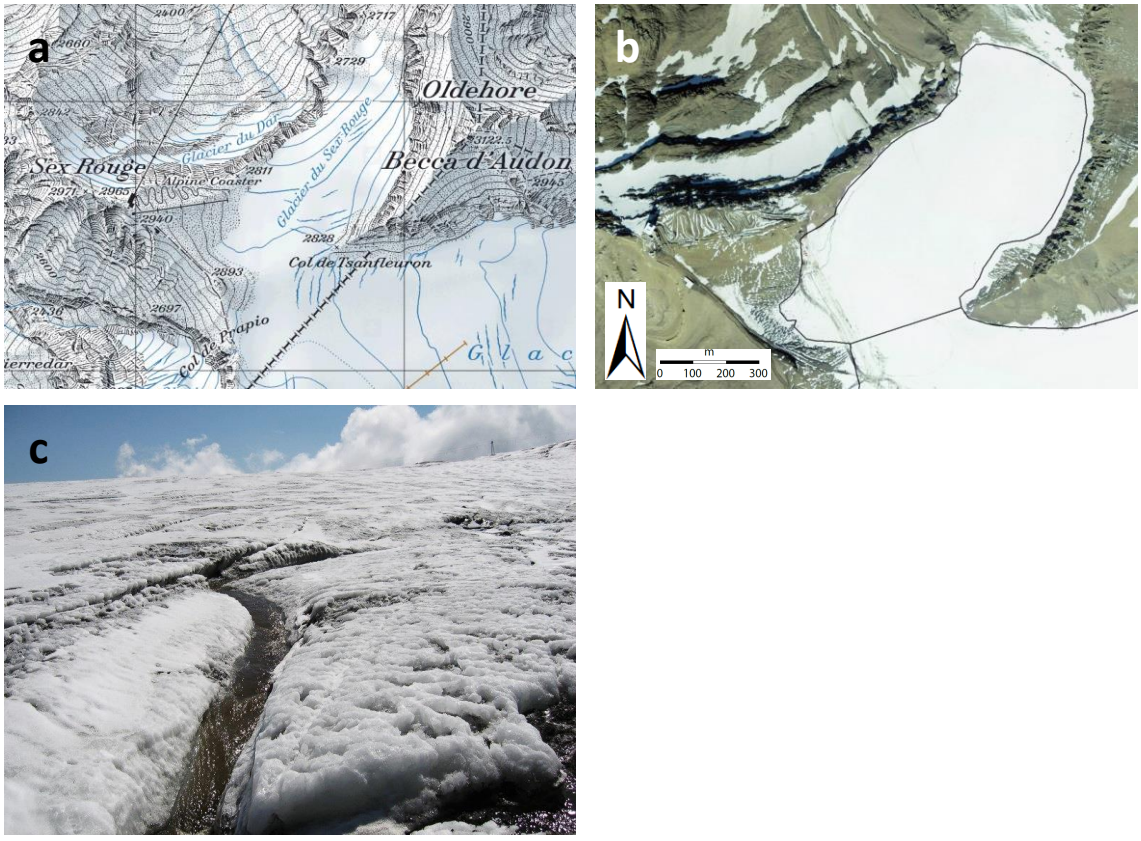

Figure 2.4: **(a)** Glacier du Sex Rouge on the Swiss national map 1:25'000 by the Federal Office of Topography swisstopo and **(b)** on the high-resolution orthophotograph SWISSIMAGE 2010. The outline is taken from the new Swiss Glacier Inventory 2010 SGI2010 (Fischer *et al.* 2014a). **(c)** Supraglacial drainage channel on Glacier du Sex Rouge 2012. The Picture was taken by A. Visinand and is printed with the permission of the photographer.

Ice thickness was measured along several GPR profiles in 2012, showing that the glacier is nearly 60 m deep at its deepest part (M. Fischer 2013, personal communication). Knowing the ice thickness distribution of Glacier du Sex Rouge, locations for two boreholes for temperature measurements were chosen by Mauro Fischer.

2.3. St. Annafirn

St. Annafirn is situated north of St. Annahorn (2937 m a.s.l.) near Gemsstock (2961 m a.s.l.). During winter, a ski slope belonging to the "Skiarena Andermatt-Sedrun" runs over parts of the small glacier, allowing easy access to the study site. At the upper part of the glacier, two little basins are attached to the glacier; one on each side (Figure 2.5). Although the area of them is small, their ice volume is not negligible. The evaluation of GPR profiles of 2013 showed, that the glacier is up to 30 m thick at the small western basin (M. Fischer 2014, personal communication).

Until today, no scientific measurements of St. Annafirn except for length changes were published. In the course of investigating very small glaciers in the Swiss Alps, four boreholes for temperature measurements were drilled into the ice by Mauro Fischer.

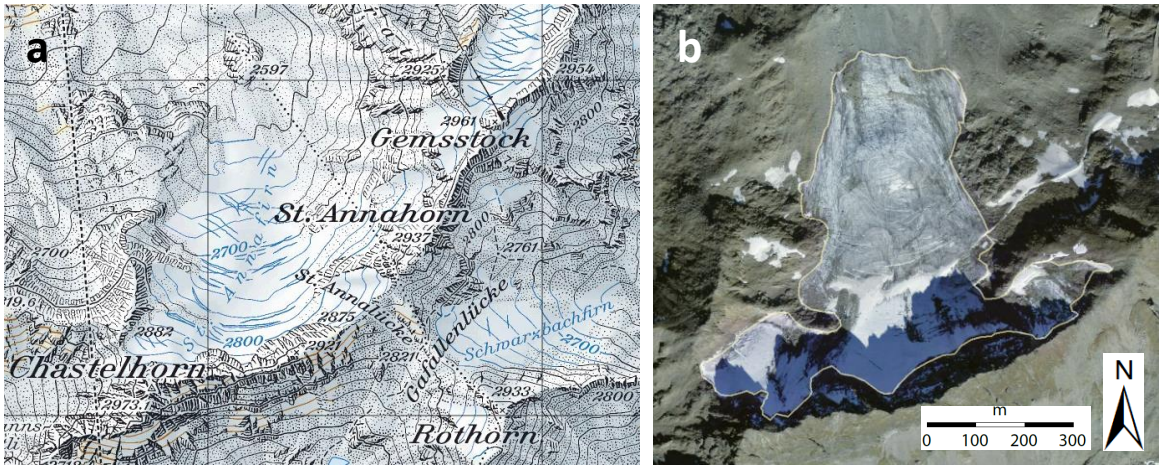

Figure 2.5: **(a)** Location of St. Annafirn in the ski area of Andermatt (UR) at the 1:25'000 Swiss national map by the Federal Office of Topography swisstopo and **(b)** on the high-resolution orthophotograph SWISSIMAGE 2010. The outline is taken from the new Swiss Glacier Inventory 2010 SGI2010 (Fischer *et al.* 2014a).

2.1. Pizolgletscher

Pizolgletscher is a steep cirque glacier protected by rockwalls on three sides (Figure 2.6a-b). It is situated at the north facing side of the Pizol summit (2844 m a.s.l.), leaving impressing moraines behind as it retreats. Mass balance observations were started in 2006 (Huss 2010).

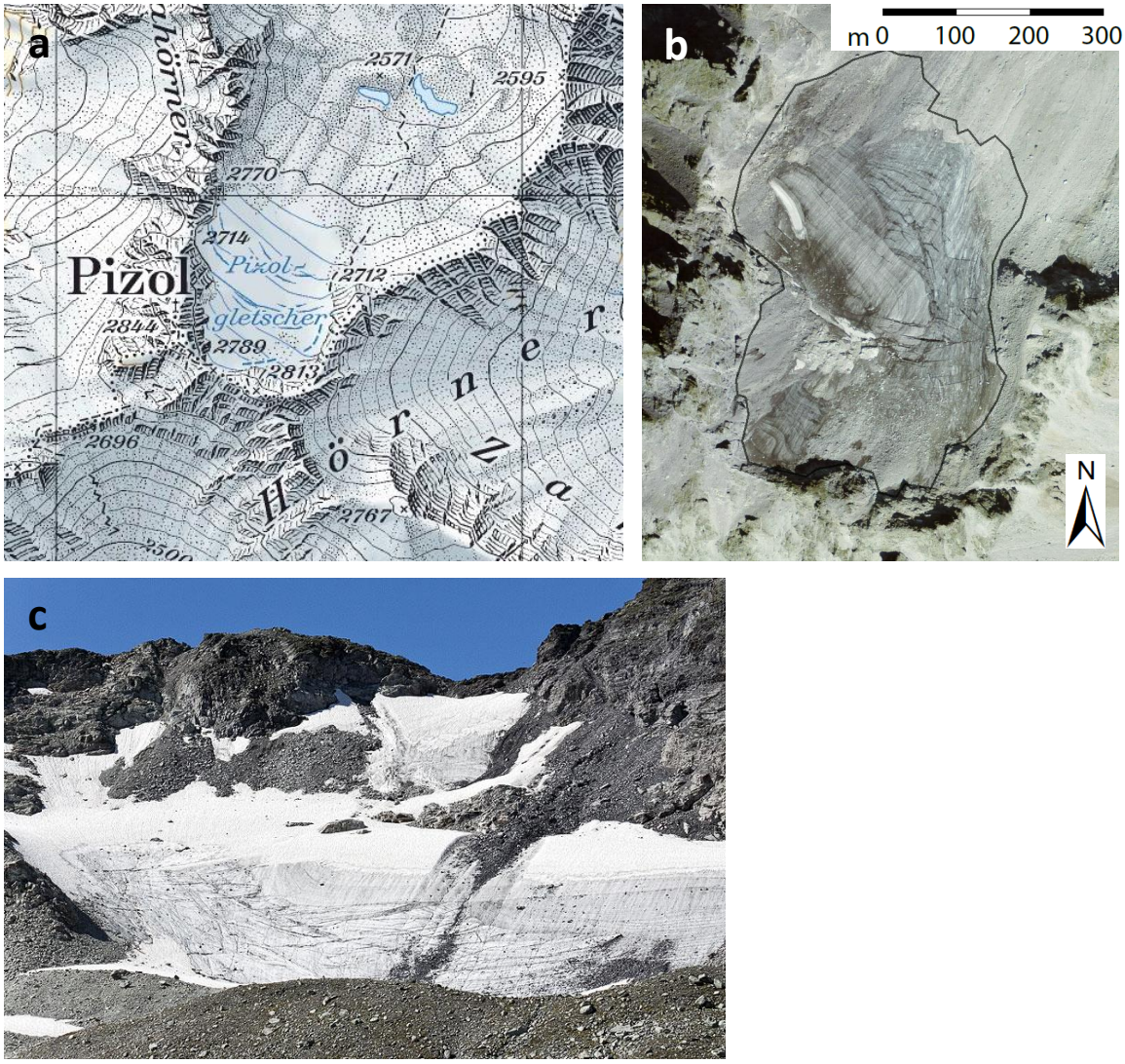

Figure 2.6: **(a)** Location of Pizolgletscher north of the summit of Pizol at the 1:25'000 Swiss national map by the Federal Office of Topography swisstopo and **(b)** on the high-resolution orthophotograph SWISSIMAGE 2011. The outline is taken from the new Swiss Glacier Inventory 2010 SGI2010 (Fischer *et al.* 2014a). **(c)** Overview of the Pizolgletscher, showing debris covering certain parts of the glacier. The Picture was taken by H. Aeschlimann in 2012 and is printed with the permission of the publisher (Glaciers online).

At the upper part of the glacier, water is flowing into crevasses and to the glacier bed, on other parts, water discharges in supraglacial channels. Pizolgletscher shows an interesting accumulation pattern, leaving the central part of the glacier as well as several parallel linear structures near the glacier terminus remaining snow-covered during summer, while the uppermost part and the steep section near the glacier terminus get snow free (Figure 2.6c). This pattern could be confirmed by direct measurements. Therefore, spatial variation of the mass balance cannot be described with altitudinal gradients like for many other glaciers. Pizolgletscher gains most of its mass at his mean elevation as well as at the glacier terminus. Thus, an advance does not take place due to a dynamic reaction of the ice mass as at larger glaciers. (Huss 2010)

3. Datasets

As all of the selected four glaciers are implemented in the PhD project of Mauro Fischer, a certain amount of measurements is already available for each glacier. An overview thereof is given in Table 3.1.

Table 3.1: Overview of available data of the four glaciers.

Glacier	Available field data
Vadret dal Corvatsch	- Temperature measurements 1999-2002 at several boreholes (Hager 2002) - Radar profiles (Busarello 2002) - Radar profiles covering the whole glacier in 2013 - Mass balance measurements since 2012
Sex Rouge	- Running temperature measurements in two boreholes (10 m and 35 m) - Radar profiles in 2010 - Radar profiles in 2012 - Mass balance measurements since 2012
St. Annafirn	- Running temperature measurements in four boreholes (8 - 10.3 m) - Radar profiles in 2012 - Radar profiles in 2013 - Mass balance measurements since 2012
Pizolgletscher	- No temperature measurements planned - Radar profile in 2010 - Mass balance measurements since 2012

Since 2012, mass balance is measured at all four glaciers. Temperature measurements are carried out at Glacier du Sex Rouge and St. Annafirn. No permanent loggers were installed as temperatures below 10-20 m are expected to show no major seasonal variability (e.g. Suter and Hoelzle 2002). Thus, sporadic reading out is assumed to be representative for ice temperatures over one or more years at a depth of several meters.

3.1. Ice temperature measurements at Glacier du Sex Rouge and St. Annafirn

At Glacier du Sex Rouge and St. Annafirn, a total of six boreholes were installed for ice temperature measurements by Mauro Fischer (Table 3.2). In all six boreholes thermistor chains of the type Thermistors YSI 4460031 with different lengths were used.

Table 3.2: Location, depths, installation and measurement dates of the boreholes at Glacier du Sex Rouge and St. Annafirn.

Glacier	ID	Location [CH1903]	Depth [m]	Installation date	Measurement date	Further information
Glacier du Sex Rouge	1	582608 N 130600 E	35	14.09.2013	17.11.2013	Located at the deepest part of the glacier
Glacier du Sex Rouge	2	582582 N 130754 E	10	14.09.2014	11.09.2014	
St. Annafirn	6	688857 N 161213 E	8	27.09.2013	04.09.2014	Located at the western little basin
St. Annafirn	9	689086 N 161690 E	10.2	03.10.2013	04.09.2014	Located at the glacier tongue

At Glacier du Sex Rouge, two boreholes were drilled in September 2013; one on the thickest middle part with a borehole depth of 35 m and one downstream towards the margin with a borehole depth of 10 m. The exact locations of the boreholes can be seen in Figure 3.1a, the coordinates and further information is provided in Table 3.2.

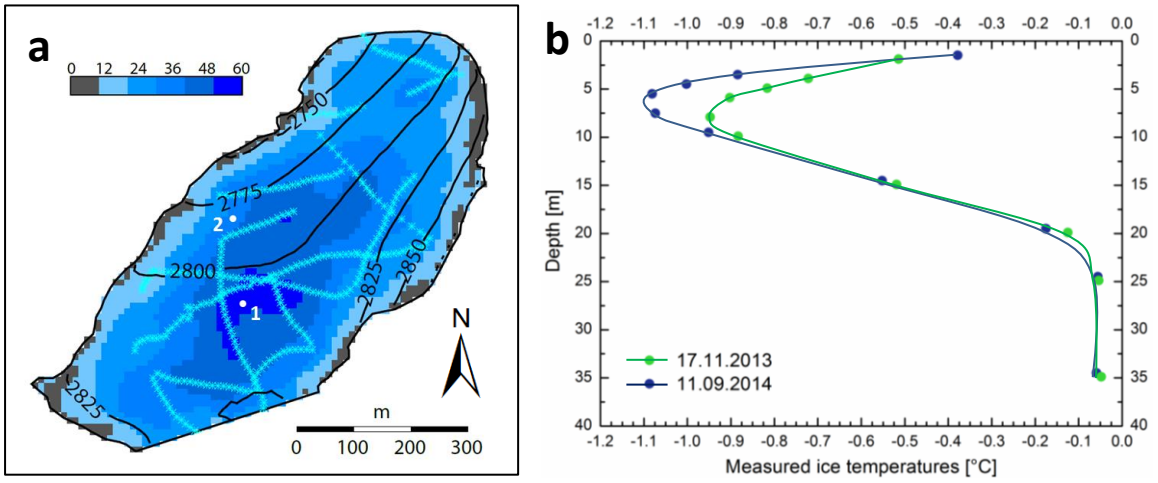

Figure 3.1: **(a)** Locations of the boreholes at Glacier du Sex Rouge. Borehole 1 is 35 m, borehole 2 is 10 m in the ice. **(b)** Measured ice temperatures at borehole 1 and 2, read out on 17.11.2013 and 11.9.2014 by Mauro Fischer.

Temperatures of borehole 1 were read out in November 2013, while to that time borehole 2 was already snowbound. The measurements show cold ice in the upper part of the glacier; the lowest measured value is -0.95°C at a depth of 7.9 m in the ice (Figure 3.1b). On 11.9.2014 both boreholes were read out again, showing slightly lower temperatures for borehole 1 (Figure 3.1b). At borehole 2, -1.16°C were measured at a depth of 9.7m.

At St. Annafirn four boreholes were drilled in September 2013 and thermistor chains were installed; all between 8 and 10.3 m deep in the glacier ice. The exact locations of the boreholes are provided in Figure 3.2 and the coordinates and further information is given in Table 3.2.

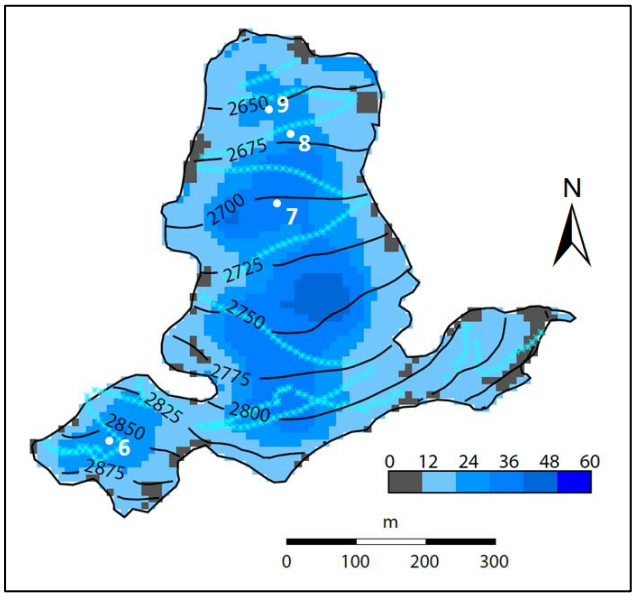

Figure 3.2: Locations of the boreholes on St. Annafirn. All four boreholes are between 8 and 10.3 m deep.

Temperatures of boreholes 6 and 9 were read out on 4.9.2014. At borehole 6 at the western little basin, -1.27°C were measured 7.24 m in the ice. At borehole 9 at the glacier tongue, -0.29°C were measured in a depth of 8.35 m. Unfortunately no measurements are available for boreholes 2 and 3 most probably due to logger breakdowns.

3.2. Ice temperature measurements at Vadret dal Corvatsch

At Vadret dal Corvatsch ice temperature measurements were already performed from 1999-2001. At these study sites mini loggers were installed at 12 boreholes with a maximum depth of 18 m. The locations of the boreholes are shown in Figure 3.3a. Ice temperatures of -6 to -1°C were measured (Figure 3.3c). Another seven loggers were installed in the rocks around the glacier to confirm permafrost (Hager 2002, Haeberli *et al.* 2004).

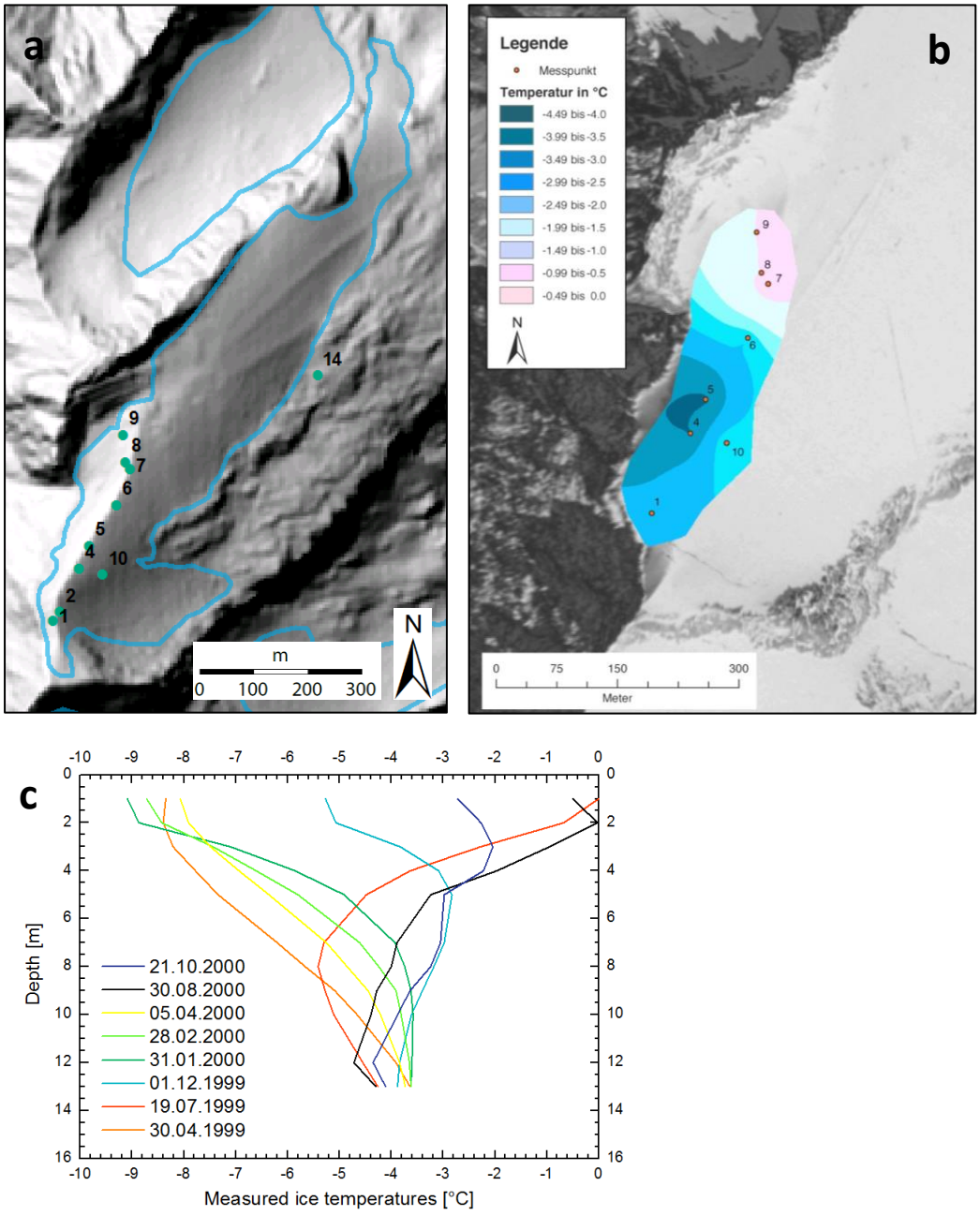

Figure 3.3: **(a)** Locations of the boreholes at Vadret dal Corvatsch shown with green dots. The blue line shows the glacier outline according to the new Swiss Glacier Inventory 2010 (Fischer *et al.* 2014a), on top of the ALTI^{3D} hillshade image (swisstopo). **(b)** Extrapolation of measured borehole temperatures at a depth of 8 m at Vadret dal Corvatsch in 2001 using the topogrid method (Hager 2002). **(c)** Measured ice temperatures of borehole 5 at different dates (Hager 2002).

3.3. Radar profiles

Several radar profiles are available for very small glaciers. All analysed radar profiles plus further information are listed in Table 1.1. For all measurements, the MALÅ ProEx + Monitor GPR system was used. Except for the Glacier du Sex Rouge 2010 and Pizolgletscher 2010 GPR surveys (Matthias Huss), GPR data shown in Table 3.3 was compiled by Mauro Fischer.

Table 3.3: Acquisition date, frequency, and GPR information for the different glaciers.

Glacier	Acquisition date	Frequency
Vadret dal Corvatsch	February 2013	100 MHz
Glacier du Sex Rouge	April 2010	25 MHz
Glacier du Sex Rouge	April 2012	50 MHz
St. Annafirn	March 2012	50 MHz
St. Annafirn	March 2013	100 MHz
Pizolgletscher	February 2010	100 MHz

3.4. Mass balance measurements

Winter accumulation and summer ablation are measured since 2012 at all four glaciers by Mauro Fischer. For Pizolgletscher, such measurements were carried out since 2008 by Matthias Huss. Some selected interpolations of field measurements for St. Annafirn and Pizolgletscher are given in Figure 3.4.

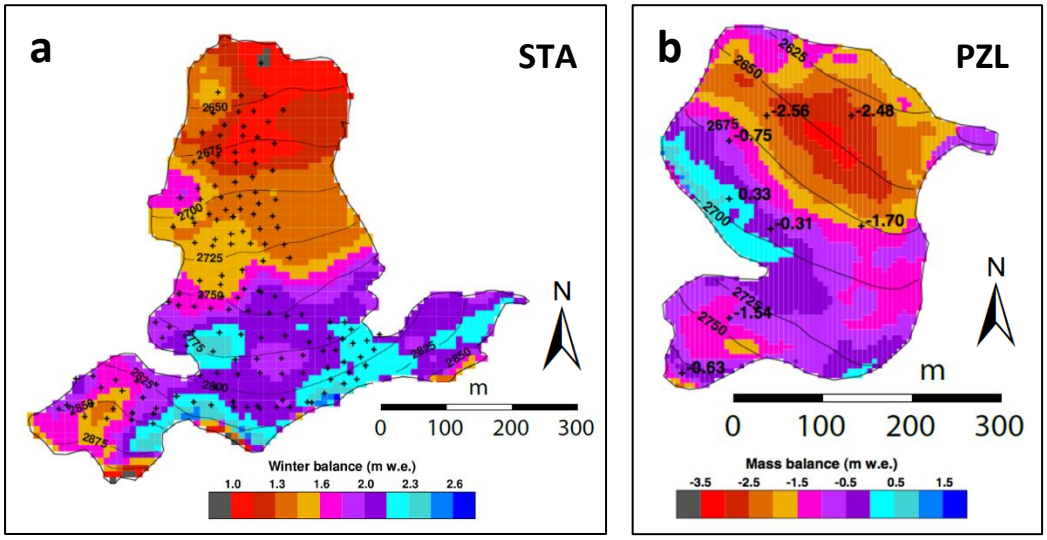

Figure 3.4: **(a)** Winter mass balance 2013/2014 on St. Annafirn and **(b)** annual mass balance 2011/2012 on Pizolgletscher, interpolated from measured accumulation (indicated by crosses) by Mauro Fischer.

3.5. Ice volume changes

Ice volume changes were derived by combination of DEMs acquired at different dates were acquired by Fischer et al. (2014b). The DHM25 Level 1 DEMs acquired from 1961 to 1991 over glacierized areas were combined with the 1973 glacier inventory and then compared to the swissALTI^{3D} DEMs from 2008–2011 and glacier outlines from the new Swiss Glacier Inventory SGI2010.

3.6. Glacier topography and glacier outlines

Glacier topography DEMs by Fischer *et al.* (2014b) derived from swissALTI^{3D} DEMs are available for all glaciers. For Pizolgletscher, additional glacier topography derived from aerial photographs taken in the years 1968, 1973, 1979, 1985, 1990, 1997 and 2006 are available. Glacier outlines from the new Swiss Glacier Inventory SGI2010 (Fischer *et al.* 2014a) are available for all glaciers.

3.7. Meteorological data

For Vadret dal Corvatsch, temperature and precipitation data is available from the SwissMeteo weather station located at the upper cable car station Corvatsch, right beside the glacier.

At Glacier du Sex Rouge, there is a close-by weather station, but unfortunately no continuous data is available from there. Temperature values are available from Les Diablerets Village, precipitation values are available from the SwissMeteo station at Château-d'Oex.

For St. Annafirn, temperature data from the SwissMeteo station "Gütsch" located above the village of Andermatt, and precipitation data from Andermatt are available.

The closest MeteoSwiss weather station with comparable elevation for Pizolgletscher is located at Säntis, which is about 32 km linear. Precipitations data is available from the SwissMeteo station at Weisstannen.

4. Methods

4.1. Modelling ice temperatures with GERM

Ice temperatures were modelled using the Glacier Evolution Runoff Model (GERM) designed by Matthias Huss. It has been used in former studies to model mass balance and runoff projections (e.g. Huss *et al.* 2008, 2010, Farinotti *et al.* 2012), but was not before used to model ice temperatures. The structure of the model will be explained first, followed by the description of the used input data, the proceeding of the calibration and a description of applied future climate scenarios.

GERM is a fully distributed glacio-hydrological model; all variables are calculated at each grid point. The model is adapted to high-mountain areas and it works well at grid sizes of 10x10m or 25x25m. It was written in IDL and it consists of different modules which are repeated in different loops (Figure 4.1).

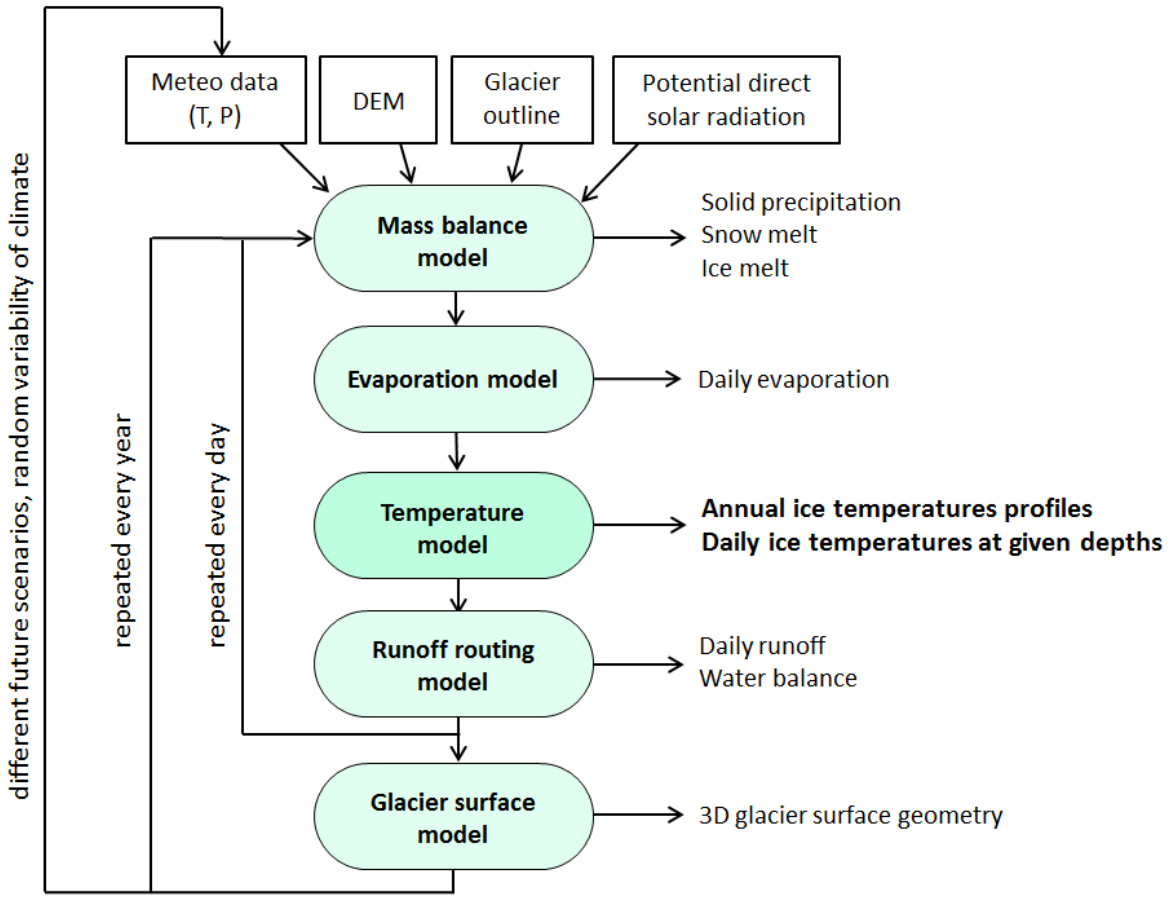

Figure 4.1: Schematic overview of GERM for the calculation of ice temperatures (modified from Huss *et al.* 2008).

With the input of a glacier bed and a glacier surface DEM, the glacier outlines, as well as daily temperature and precipitation data, the model calculates the solid precipitation and the melt of snow and ice. Therewith, the mass balance, the ice volume change and the snow depth can be generated and information on the glacier surface geometry can be updated in an implemented module (Huss et al. 2008). In a further step, englacial temperatures are modelled three-dimensionally. Different points in space can be defined, where the model calculates vertical ice temperature profiles as well as daily temperature series at specified depths.

4.1.1. Mass balance model

Melt is calculated using a simplified energy balance model according to Oerlemans (2001):

$$E = d\,(1 - \alpha)Q_e + C_0 + C_1 \cdot T_a \qquad (1)$$

where d is a reduction factor for incoming shortwave radiation which accounts for cloudiness or haze, α is the albedo of the surface, Q_e is the clear-sky shortwave radiation, and $C_0 + C_1T_a$ is the sum of the longwave radiation balance and the turbulent heat fluxes (Machguth *et al.* 2006).

As recommended by Oerlemans (2001) and done so in former modelling approaches (e.g. Machguth *et al.* 2006), C_1 was set to 10 Wm^{-2} and C_0 was used as a tuning factor. Potential radiation was calculated beforehand on behalf of a DEM of the surrounding area. Different albedos were set for snow, firn and ice.

The energy balance model has the advantage that despite its physical basis, it only needs few, often easily accessible input data as daily temperature and precipitation values of a nearby weather station. GERM accounts for altitude differences of the location of the weather station and the glacier using a temperature gradient of -0.65°C/100 m and a precipitation gradient of 1%/100 m. Additionally, a precipitation correction factor (c_prec) was introduced accounting for other effects influencing the precipitation like exposition or wind. Additionally, avalanching and wind drift effects are accounted for by small-scale effects of snow redistribution by means of the input DEM. Snow accumulation decreases linearly between 40° and 60° from 100% to 0%, and cells with a concave curvature receive more accumulation than those with convex curvature (Huss *et al.* 2008a).

4.1.2. Glacier evolution model

As nowadays virtually all glaciers in the Swiss Alps are out of equilibrium and are losing mass and area, the glacier surface needs to be updated regularly. The total surface area, on which melt can occur has a strong impact on the runoff regime. In GERM, the surface update is generated using the mass conserving Δ*h*-parameterization that was initially proposed by Huss *et al.* (2008). The Δ*h*-parameterization is a function relating the elevation of the glacier surface *h* to the surface elevation change Δ*h* (equivalent to ice thickness change) occurring over a given time (Huss *et al.* 2010c).

There are different options for the Δ*h*-parameterization implemented in GERM. For local Δ*h*-parameterization, the redistribution of the ice volume change is executed according to a pattern derived from direct observations (Huss 2011). This option is only available for a few glaciers with an additional input file and was not used in this study.

Empirical Δ*h*-parameterization is possible for any glacier. Therefore, generalized functions have been derived for three different size classes (Figure 4.2). Here obviously the size class "small" was used.

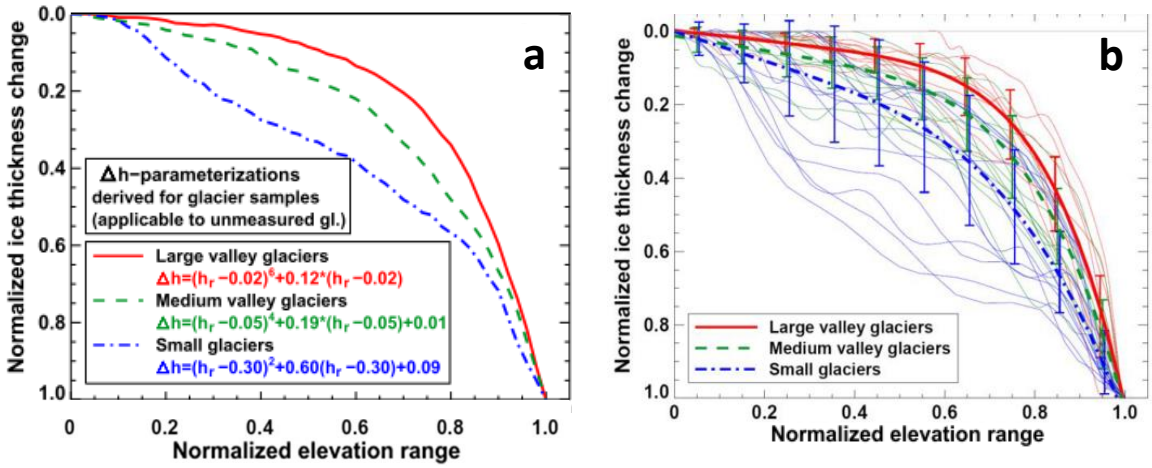

Figure 4.2: **(a)** Empirical Δ*h*-parameterizations for three glacier size classes applicable to unmeasured glaciers derived from digital elevation model comparison for 34 glaciers. The equations refer to a numerical approximation of the line for each size class. **(b)** Approximations including individually derived parameterizations for all 34 glaciers (thin lines). The colour indicates the size class. Error bars show the uncertainty of the approximation; they are calculated as the standard deviation of the individual parameterizations within the size class. (Huss *et al.* 2010c)

4.1.3. Temperature model

The temperature model was originally designed to model three-dimensional permafrost temperatures. With some modifications of soil parameters, the model was adapted to glacier ice (Huss *et al.* 2011).

The temperature model starts at the glacier surface, taking daily air temperature values as input data. Temperatures at isolated individual cells are then calculated downwards in in distinct nodes with 0.5 m distance each. To save computing time, results are only printed at specified cells. Parameters influencing the evolution of temperatures with depth are thermal conductivity and heat capacity, as well as geothermal heat flux. The model also includes processes of latent heat exchange, like thawing, freezing, and water infiltration. Since individual spatial model cells are stable, no heat advection is implemented in the model. All implemented processes are represented in Figure 4.3.

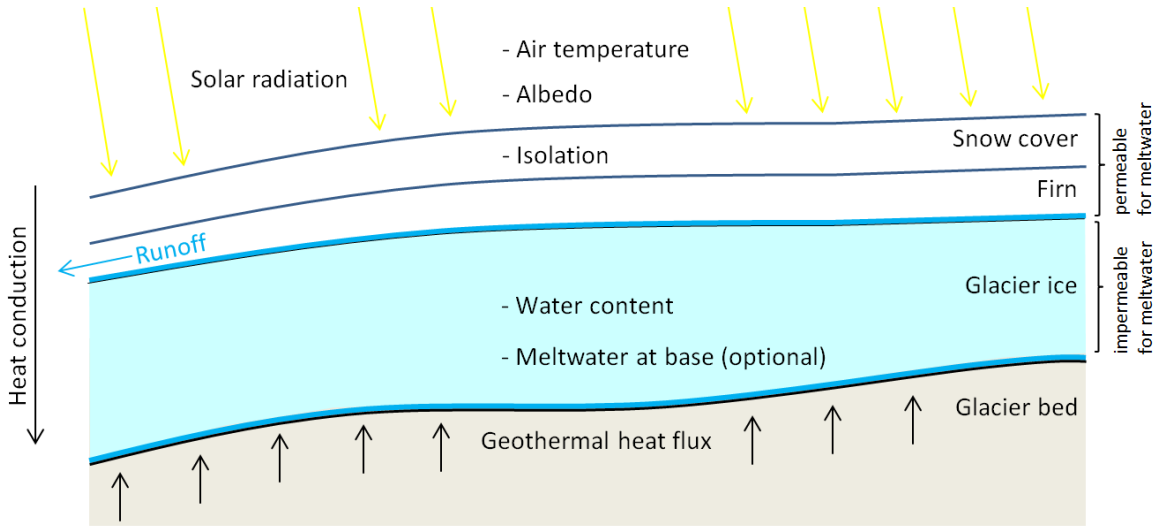

Figure 4.3: Schematic representation of the most important processes included in the temperature model (modified from Huss *et al.* (2011)).

The firn or snow cover has the capacity to store meltwater, which has a major influence on ice temperatures due to refreezing processes and the release of latent heat. For the very upper part of a glacier ice column, a value defining the porosity is defined, as well as a value for the maximum water content. If accessible ice-free pores exist, meltwater is able to penetrate the upper 0.4 m the ice. Glacier ice at greater depths is assumed to be impermeable for meltwater.

Different thermal conductivity and heat capacity values are set for ice, water and air, which coexist within the glacier. The glacier is seen as a homogeneous ice body with equal water content throughout the glacier. There is an additional feature to dictate water at the glacier base and therefore setting the ice temperature at the glacier base to 0°C.

To include the effect of the insulating firn and snow cover, a pair of threshold parameters was introduced to the model. If the snow cover is below the lower parameter, no insulation takes place and the temperature of the first glacier layer is set to the input air temperature. If the snow cover is higher than the upper threshold, the surface is fully cut off from the air temperature and the glacier surface temperature is set to 0°C. If the snow cover is within the two thresholds, the temperature of the first layer is linearly interpolated between the air temperature and 0°C (Figure 4.4).

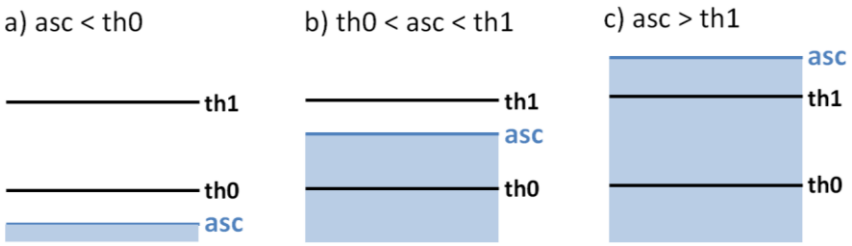

Figure 4.4: Concept of the thresholds to control the insulation of the snow cover, where th0 stands for the lower and th1 for the upper threshold and asc is short for actual snow cover.

4.1.4. Input data

For the individual glaciers, input DEMs of a different year were available. For Glacier du Sex Rouge, a 10m-resolution DEM was used, whereas the other DEMs have a spatial resolution of 25 m (Table 4.1).

Table 4.1: Information about the used input DEM for the individual glaciers.

Glacier	Year	Spatial resolution	Source
Vadret dal Corvatsch	2008	25 m	Fischer *et al.* (2014b)
Glacier du Sex Rouge	2010	10 m	Fischer *et al.* (2014b)
St. Annafirn	2004	25 m	Fischer *et al.* (2014b)
Pizolgletscher	2006	25 m	Huss *et al.* (2010a)

The sources of the used meteorological input data for the individual glaciers is listed in Table 4.2

Table 4.2: Sources of the used meteorological input data for Vadret dal Corvatsch (COR), Glacier du Sex Rouge (SER), St. Annafirn (STA) and Pizolgletscher (PZL).

Glacier	Temp.			Prec.		
	Weather station	**Altitude [m a.s.l.]**	**Location**	**Weather station**	**Altitude [m a.s.l.]**	**Location**
COR	Upper cable car station Corvatsch	3315	783155 N 143520 E	Upper cable car station Corvatsch	3315	783155 N 143520 E
SER	Input values were generated by combining data from several stations by Matthias Huss					
STA	Gütsch	2282	690140 N 167590 E	Andermatt	1423	668 310 N 165 236 E
PZL	Säntis	2490	744180 N 234920 E	Weisstannen	998	744624 N 206078 E

4.1.5. Proceeding of the model calibration

No module performing automatic calibration is implemented in the code. But thanks to the module-structure, parameters for the individual modules can be tuned step-wise by hand. Firstly, parameters regulating the mass balance were calibrated. Secondly, the parameter regulating the insulation of the snow cover was calibrated.

Because the turbulent heat flux C_1 was set to 10 Wm^{-2} – as suggested by (Oerlemans 2001) – only two parameters needed to be calibrated for the energy balance model; namely the precipitation correction factor c_prec and the parameter for longwave radiation C_0. The time period of the calculated mass balance values used for calibration as well as the calibrated parameters C_0 and c_prec for all glaciers are listed in Table 4.3. The differences in the longwave radiation may to a certain degree result from the fact that several combinations of the two calibrated factor may lead to the same mass balance results; especially for those glaciers for which no winter mass balance values are available.

The parameters of the mass balance model were calibrated so that the cumulative mass balance over the calibration period was within 5 cm w.e. and the root mean square error (RMSE) between the modelled and calculated mass balance values was minimized.

For Pizolgletscher, annual mass balance as well as winter mass balance values from Huss *et al.* (2010a) were used for calibration. There, volume changes calculated from eight DEMs (derived from aerial photographs taken in the years 1968, 1973, 1979, 1985, 1990, 1997 and 2006) and annual and winter mass balance measurements from 2006 to 2008 were combined. The fact that information about winter mass balance could be consulted helped to calibrate the parameters of the mass balance model. For Pizolgletscher, c_prec was calibrated first, making sure to achieve a good fit for the winter mass balance. While C_1 was set to 10 Wm^{-2}, C_0 was calibrated second. This parameter influences the melt and was used to adjust the annual mass balance values.

For Vadret dal Corvatsch, Glacier du Sex Rouge and St. Annafirn, volume change values derived from the comparison of DEMs of different dates by Fischer *et al.* (2014b) were used for calibration. There, the DHM25 Level 1 DEMs acquired from 1961 to 1991 over glacierized areas were combined with the 1973 glacier inventory and then compared to the swissALTI^{3D} DEMs from 2008–2011 and glacier outlines from the new Swiss Glacier Inventory SGI2010. The resulting volume changes were used to calibrate c_prec for Vadret dal Corvatsch, Glacier du Sex Rouge and St. Annafirn. C_0 was set similarly as for Pizolgletscher for these three glaciers, as here no winter mass balance values were available. All calibrated model parameters concerning the energy balance are listed in Table 4.3 for all four glaciers.

Table 4.3: Calibrated parameters regulating the energy balance – longwave radiation (C_0) and precipitation correction (c_prec) – for the individual glaciers, as well as period, source and accuracy for the mass balance or volume changes which were used for calibration.

Glacier	C_0 [Wm^{-2}]	c_prec [%]	Calibration period	Source	Accuracy
Vadret dal Corvatsch	23.38	150	1991-2009	Fischer *et al.* 2014b	±0.270 m w.e.a^{-1}
Glacier du Sex Rouge	21.9	120	1961-2010	Fischer *et al.* 2014b	±0.082 m w.e. a^{-1}
St. Annafirn	20.4	110	1986-2010	Fischer *et al.* 2014b	±0.195 m w.e. a^{-1}
Pizolgletscher	33	176.4	1990-2008	Huss *et al.* 2010a	±0.35 m w.e. a^{-1}

After the calibration of the mass balance model, the parameters of the temperature model were adjusted. As most of the ice temperature parameters are rather insensitive, the calibration was carried out only by the regulation of the snow thresholds (Figure 4.4). The thresholds were calibrated comparing measured and modelled ice temperature measurements without dictating meltwater at the glacier base. For Pizolgletscher, threshold values had to be estimated, as here no temperature measurements were available for calibration. Except for the snow thresholds, all parameters remain the same for all glaciers (Table 4.4).

Table 4.4: Parameters of the temperature model in GERM for Vadret dal Corvatsch (COR), Glacier du Sex Rouge (SER), St. Annafirn (STA) and Pizolgletscher (PZL). Where no glacier is named, the parameter remains the same for all glaciers.

Parameter	**Value**	**Unit**	**Description**
watercontmax	0.5	-	maximum water content
pliq_offset	1	°C	rain colder than air temperature (set to 100 when water infiltration should be turned off)
cond	ice 2.33 water 0.56 air 0.02	$J\ s^{-1}\ K^{-1}\ m^{-1}$	Thermal conductivity of the different materials
capacity	ice 1.89 water 4.22 air 0	$10^6\ J\ m^{-3}\ K^{-1}$	Heat capacity of the different materials
geothermal	0.03	$W\ m^{-2}$	Geothermal heat flux
snow_thresholds	COR 90, 360 SER 130, 360 STA 100, 360 PZL 100, 360	mm w.e. (snow)	Thresholds regulating the insulation of the snow cover. For detailed description see Figure 4.4
porosity	0.01	-	Porosity
porosity_depth	0.4	m	Depth in which porosity changes

4.1.6. Modelling of future climate scenarios

The possibility to perform future model runs is implemented in the code of GERM. To do so, some additional input files containing the future climate scenarios are required. Climate scenarios described by Bosshard *et al.* (2011) were used. These data was generated using a simple form of the delta change method and is available for various local stations. With the delta change method, a climate change signal is applied to observed climate data. Thus, the obtained series of temperature and precipitation at daily resolution show annual cycles. (Huss *et al.* 2008b)

All climate scenarios were driven by the A1B scenario (Nakicenovic and Swart 2000), representing the midrange of the greenhouse gas scenario. Here, mainly a medium scenario was applied (MPI_ECHAM5_REMO). For comparison of the evolution of ice temperatures in the future, a high and a low medium were applied. Further information on these scenarios is provided in Table 4.5 and in Huss *et al.* (2014).

Table 4.5: Information about the different applied regional climate scenarios of the ENSEMBLES project with the responsible institution and abbreviations for the Global Circulation Model (GCM) and the Regional Climate Model (RCM) used. Projected changes in mean winter (November–April) and summer (May–October) air temperature ΔT_W and ΔT_S, and precipitation ΔP_W and ΔP_S. (Huss *et al.* 2014)

Scenario	Institution	GCM	RCM	Reference in GERM	ΔT_W [°C]	ΔT_S [°C]	ΔP_W [%]	ΔP_S [%]
High	ETHZ	HadCM3Q0	CLM	Scenario 2	+3.51	+4.60	+6	+2
Medium	MPI	ECHAM5	REMO	Scenario 5	+3.69	+4.04	+6	-10
Low	SMHI	BCM	RCA	Scenario 10	+2.23	+2.79	-11	-11

4.1.7. Execution of model runs

All model runs were initiated in the year 1980 and run until the end of the future lifetime of the individual glaciers. Since the input DEMs are of specific dates, model runs of the past years were carried out assuming no glacier change. The Δh-parameterization to account for mass changes was initiated at the year of the input DEM (Table 4.1).

4.2. Analysis of GPR profiles

Radio detecting and ranging (radar) is a useful technique to detect objects by sending out electromagnetic waves and analysing the backscatter of the sent signals. Ground penetrating radar (GPR) is a non-distractive geophysical method to interrogate layers of different dielectric properties in the ground and is nowadays widely applied in glaciology; for example to detect the glacier bed, areas of different water content or a change in the thermal regime within the glacier ice (e.g. Pettersson *et al.* 2003, Eisen *et al.* 2009).

4.2.1. Theoretical background on GPR

GPR consists of a sending and a receiving antenna. The sending antenna emits electro-magnetic energy, which penetrates the ground. This signal is then eventually reflected at inhomogeneities in the ground. The receiving antenna registers the resulting backscatter and the travel time of the signal. Together with the travel time and the typical radar wave velocity within a certain medium, the distance to the reflector can be calculated (Figure 4.5). The sending antenna collects the incoming signals in so-called "samples", which represent the amplitude and the phase of the signal in a certain time interval. A series of measurements at a single point, consisting of many "samples", is called "trace" (Murray *et al.* 2000).

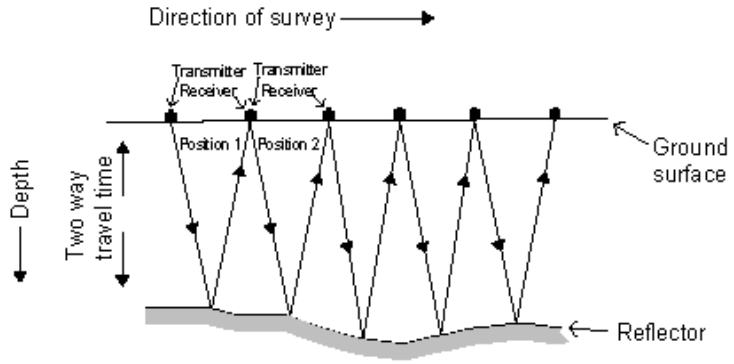

Figure 4.5: Schematic overview of the functionality of GPR (modified from Jol and Smith (1991)).

The signals registered at the receiving antenna are plotted vertically according to their arrival time. However the arrival time of the signal on an isolated track doesn't reveal any information about the direction of the reflector (Figure 4.6). Nevertheless it is possible to calculate the source direction of a reflected signal if their neighbouring samples are analysed. The transformation of the apparent reflexion points to the real reflectors is called migration (Wagner 1996).

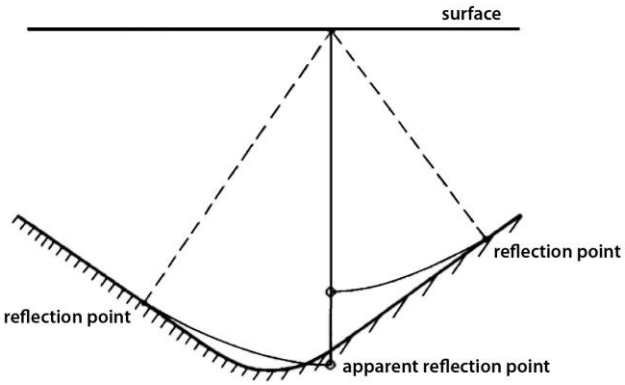

Figure 4.6: As radar signals are emitted three-dimensionally, the first signal might origin from a reflector that is not vertically underneath the point, were the signal has been sent. (translated from Wagner (1996))

Accurate determination of the radar wave velocity v is fundamental to radar-derived distance measurements, as it defines the relationship between the two-way travel time (Δt) of the recorded signal and the depth (h) in the host medium (Reynolds 2011):

$$\Delta t = \frac{2h}{v} \qquad => \qquad h = \frac{\Delta t \cdot v}{2} \tag{2}$$

The velocity of propagation of radar waves (v) varies in different media. In dry ice, a velocity of 0.168 m/ns is typical, while lower speeds are typical are typical for ice containing a certain amount of liquid water (Murray *et al.* 2000, Gusmeroli *et al.* 2010).

The accuracy of GPR measurements depends on the frequency and polarisation of the radar signal, the contrast of the electromagnetic properties, the size, shape and geometry of the target object, and the receiver frequency. Objects with a simple geometry can be detected up to a size of about 1/3 of the actual wavelength, if the contrast to the enclosing medium is great enough (Nguyen 1999). Different frequencies of the antennae are chosen considering the purpose of the resulting image. Low frequencies are used for high penetration depth with less resolution – for example to detect the glacier bed, while high frequencies result in better resolution but lower penetration depth. Therefore, the choice of the frequency is always a trade-off between resolution and penetration depth (Vonder Mühll 1993).

Frequencies of 1 to 900 MHz are possible in glaciology, as in this range, snow and ice is penetrated well. Antennae of 25, 50, 100 or 150 MHz are widely used for investigations at glaciers (e.g. Gilbert *et al.* 2012, Zhang *et al.* 2013). Usually, a bistatic – meaning with two antennae – radar system is carried over the glacier. An additional GPS (Global Positioning System) registers the position of the tracks and the acquired samples can be geo-referenced automatically.

4.2.2. Processing of the GPR data

The raw data of the given radar profiles was processed using the program ReflexW (Version 7.2.3) by K. J. Sandmeier. Detailed description of each processing step can be found in the manual of the program (Sandmeier 2013). A velocity of 0.167 m/ns was used for the conversion from two way travel time to distances. This value was chosen because it is assumed to be a good compromise between velocities in dry and in wet ice. Since no glaciers with great depths were analysed and thus errors don't propagate far, no change of the velocity was undertaken.

For those measurements where GPS data was available, equidistant traces were made. This accounts for the distortion resulting from irregular walking velocities and interpolates the data to the given "trace increments". The units of the x-axis should now be true. Then, a frequency band-pass filter was applied to the data. All frequencies outside a defined range are eliminated from the data, so that only the frequencies of interest are kept and enhanced. If the data showed horizontal lines that are no real reflectors, the "background removal"-filter was applied. This filter subtracts the average in x-direction of each trace. However, if a real horizontal reflector exists, this might vanish. The "background removal"-filter was applied to nearly all given profiles.

As the first signal arriving at the receiving antenna results from the direct radar wave travelling through the air or at the surface, it doesn't carry any information about the ground. It is thus to be eliminated through a static correction, the so-called function of "shift to zero". This changes the reference surface and therefore shifts the depth-axis. Due to several reflections of the radar signal in the ground, the backscatter of the signal gets weaker with the penetrated depth. The "gain function" counteracts to this effect as the signal strength is enhanced with depth. In ReflexW, a linear and an exponential parameter can be chosen to control the magnitude of the gain. To account for distortion caused by an irregular reflector surface, several migration filters are available in ReflexW. Here, the "Kirchhoff 2D migration"-filter was applied to all profiles.

After the completed radar data processing, quantitative information can be extracted by picking. Thereby, reflectors can be marked and the data exported, e.g. to visualize them a geographic information system (GIS).

5. Results

5.1. Modelled ice temperatures with GERM

5.1.1. Comparison of modelled and measured borehole temperatures

For Glacier du Sex Rouge and St. Annafirn, modelled ice temperatures could be compared to recently (2013 and 2014) measured borehole temperatures. For each measured value, the respective modelled value of the same year and approximately the same depth was plotted in the same graph (Figure 5.1).

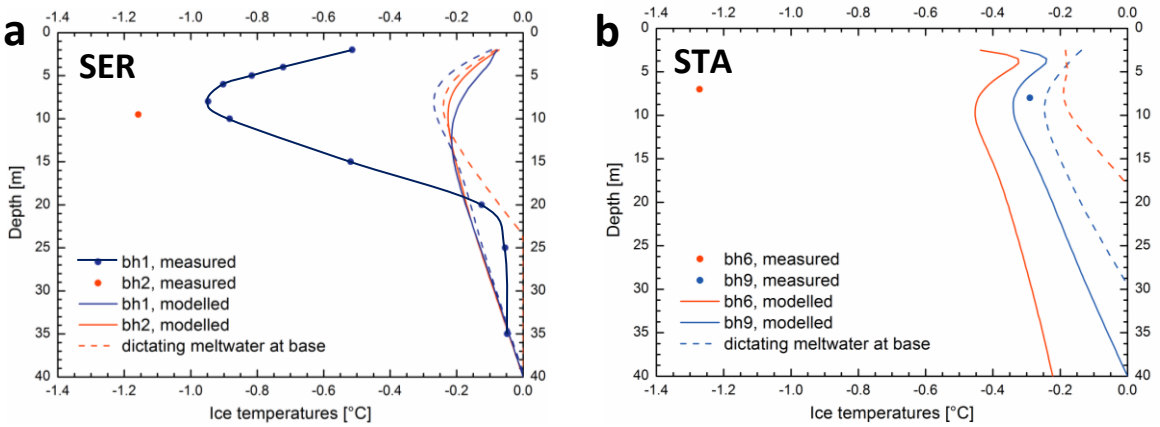

Figure 5.1: Measured (dots) and modelled (lines) ice temperatures for the year 2014 of **(a)** Glacier du Sex Rouge (SER) and **(b)** St. Annafirn (STA) at different boreholes. For both glaciers and boreholes, two scenarios are plotted: Once assuming meltwater at the glacier base (dashed line) and once without assuming meltwater at the glacier base (sold line).

At Glacier du Sex Rouge, differences in modelled ice temperatures of the two borehole locations are underrepresented. At a depth of 10 m, differences in modelled ice temperatures are around 0.01°C, whereas ice temperature differences at similar depth were measured to be 0.12°C.

At St. Annafirn, modelled ice temperatures show a difference of 0.06°C (no meltwater dictated at the glacier base) or 0.03° (meltwater dictated at the glacier base). Measured ice temperatures at similar depth show a difference of 0.98°C. Depending whether meltwater is dictated at the glacier base or not, temperatures for borehole 6 were even modelled higher than the ones for borehole 9.

For Vadret dal Corvatsch, only some older measurements (1999-2001) by Hager (2002) were available for comparison. A comparison of measured and modelled ice temperatures in 2001 was carried out for 6 boreholes. Differences between the two scenarios (with or without dictating meltwater at the glacier base) are greatest where ice temperatures are lowest and where glacier thickness is smallest (Figure 5.2). The locations of the boreholes is given in Figure 3.3.

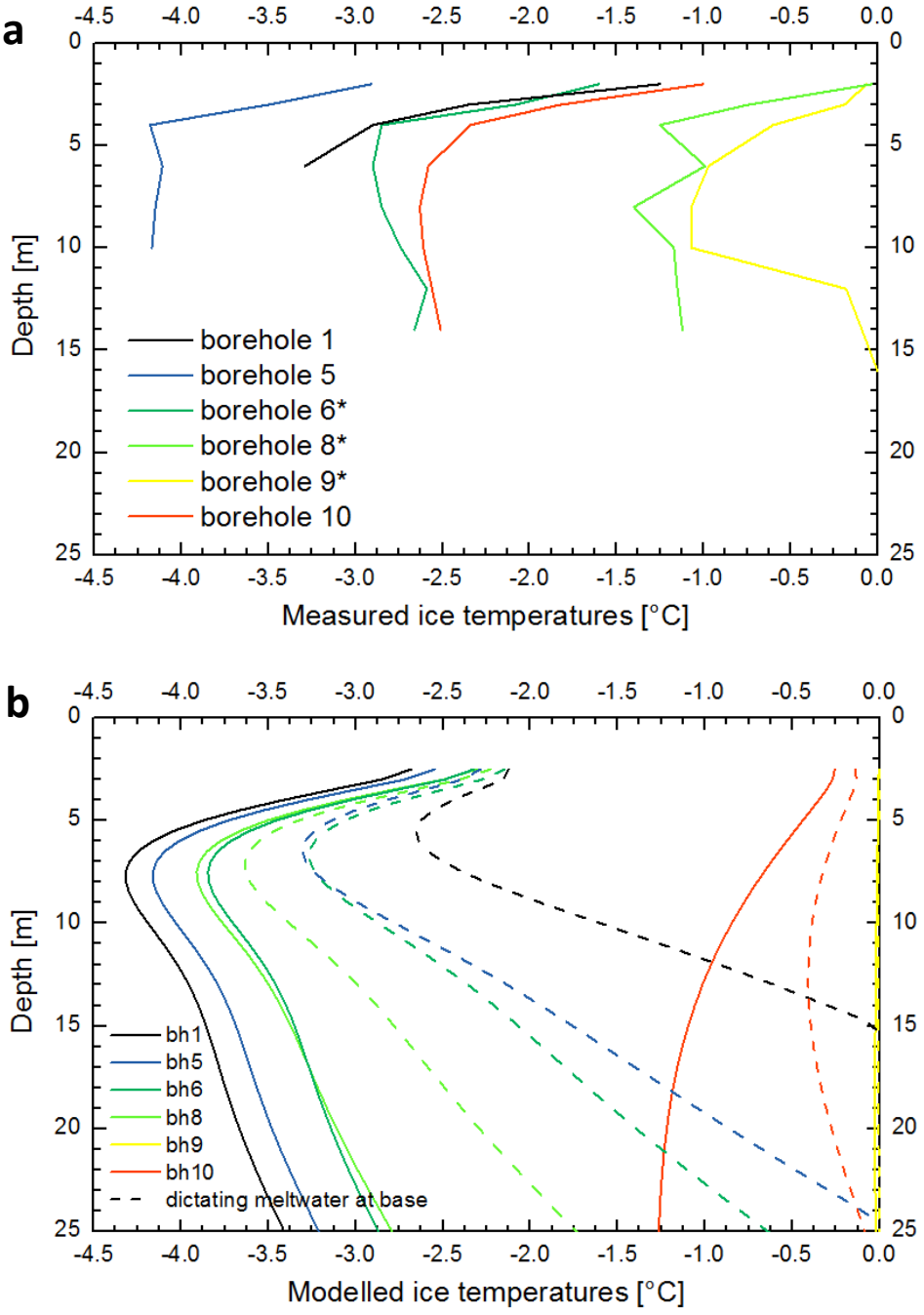

Figure 5.2: **(a)** Measured* and **(b)** modelled ice temperatures of Vadret dal Corvatsch for the year 2001 at different boreholes. For each borehole, two scenarios are plotted: Once assuming meltwater at the glacier base (dashed line) and once without assuming meltwater at the glacier base (sold line).

* for marked boreholes measured temperatures were linearly extrapolated (Hager 2002)

The comparison of ice temperatures of the upper 10-15 m is critical, as here the annual cycle is prevailing. Thus, lowest measured ice temperatures were compared to modelled values. Best fit between modelled ice temperatures and field data is given for borehole 5 if the model doesn't dictate meltwater at the glacier base. Least agreement could be found for temperatures at borehole 8, where modelled ice temperatures are 2.5°C below measured values. No spatial trend of better fits could be found.

At borehole 5 at Vadret dal Corvatsch, measurements were carried out at several dates in the year 1999 and 2000 (Hager 2002). The comparison of measured and modelled ice temperatures show, that modelled values show less annual amplitude. Measured 3m-temperatures show a difference of almost 8°C from lowest (-8.21°C on 30.4.1999) and to highest value (-0.95°C on 30.8.2000). The lowest modelled 3m-temperature was -6.4°C for the 30.4.1999 and the highest one -3.2°C for the 21.10.1999. Thus, modelled 3m-temperatures only show a range of 3.2°C. The modelled ice temperatures show inner-annual differences of less than 0.2°C at a depth of 10 m, whereas the measured temperatures at the same depth vary by 1.5°C (Figure 5.4). Therefore it can be assumed that real ice temperature show bigger annual cycle than modelled ones.

At borehole 5 at depth of 3 m, lowest temperatures are usually modelled for March-April, at a depth of 6 m in June. The same pattern can be found at the measured temperatures.

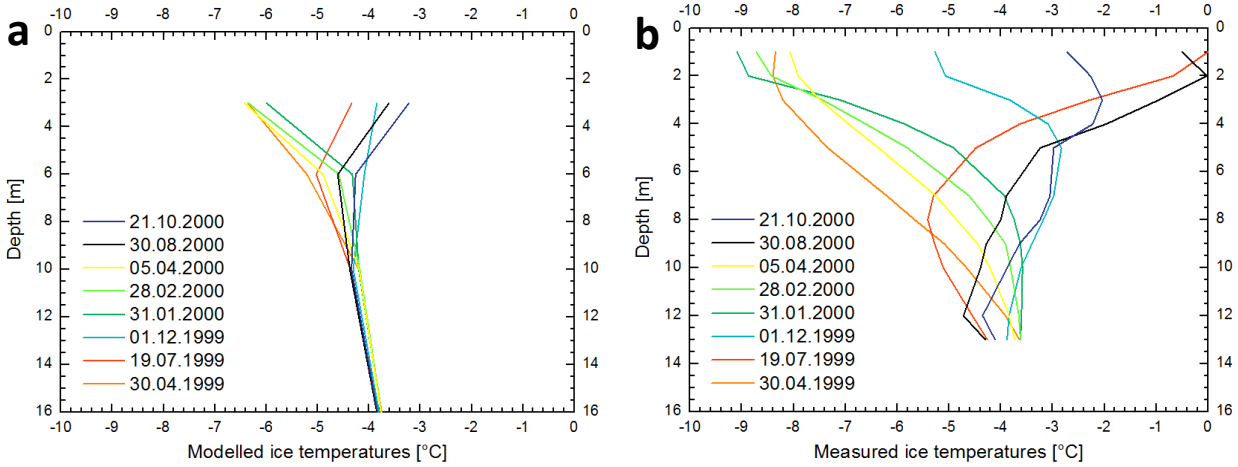

Figure 5.3: **(a)** Modelled ice temperatures over the year compared to **(b)** measured temperatures of the same dates in the years 1999-2000 by (Hager 2002).

An overview of further comparisons of measured and modelled borehole temperatures of Vadret dal Corvatsch, Glacier du Sex Rouge and St. Annafirn is given in Table 5.1. Where no recent meteo data was available yet (years 2013 and 2014), the future scenario 5 was applied to generate the data. For each borehole, the model was run once with and once without dictating meltwater at the glacier base. The scenario resulting in better fit with the measured values is highlighted with bold letters.

Table 5.1: Comparison of selected measured ($T_{meas.}$) and modelled ($T_{mod.}$) borehole (bh) ice temperatures at Vadret dal Corvatsch (COR), Glacier du Sex Rouge (SER) and St. Annafirn (STA). For modelled temperatures, future scenario 5 was applied as no meteo data for the running years 2013 and 2014 were available yet. For each borehole, the model was run once with and once without dictating meltwater at the glacier base. The scenario resulting in better fit with the measured values is highlighted with bold letters.

Glacier	bh	Year	Depth [m]	$T_{meas.}$ [°C]	Depth [m]	$T_{mod.}$ [°C]	Simulating meltwater at base	$T_{meas.}$- $T_{mod.}$ [°C]
COR	1	2001	6	-3.29	6.0	-4.162 **-2.64**	No **Yes**	0.872 **-0.65**
COR	5	2001	10	-4.17	10.0	**-4.029** -2.774	**No** Yes	**-0.141** -1.396
COR	10	2001	14	-2.51	14.0	**-1.058** -0.404	**No** Yes	**-1.452** -2.106
SER	1	2013	7.9	-0.948	8.0	-0.188 **-0.269**	No **Yes**	-0.76 **-0.679**
SER	1	2013	24.9	-0.054	25.0	-0.129 **-0.121**	No **Yes**	0.075 **0.067**
SER	2	2014	9.7	-1.158	9.5	-0.226 **-0.238**	No **Yes**	-0.932 **-0.92**
STA	6	2014	7.24	-1.272	7.5	**-0.426** -0.19	**No** Yes	**-0.846** -1.082
STA	9	2014	8.35	-0.290	8.3	-0.337 -0.243	No Yes	-0.047 0.047

As only a limited amount of borehole temperature measurements are available, it is difficult to quantify the uncertainty of modelled data.

5.1.2. Spatial distribution of modelled ice temperatures

For Vadret dal Corvatsch, lowest ice temperatures were modelled where the ablation is highest (Figure 5.4). For Glacier du Sex Rouge, St. Annafirn and Pizolgletscher, the spatial distribution of modelled ice temperatures is barely visible, as differences in values are within the class sizes (Figure 5.5-5.7).

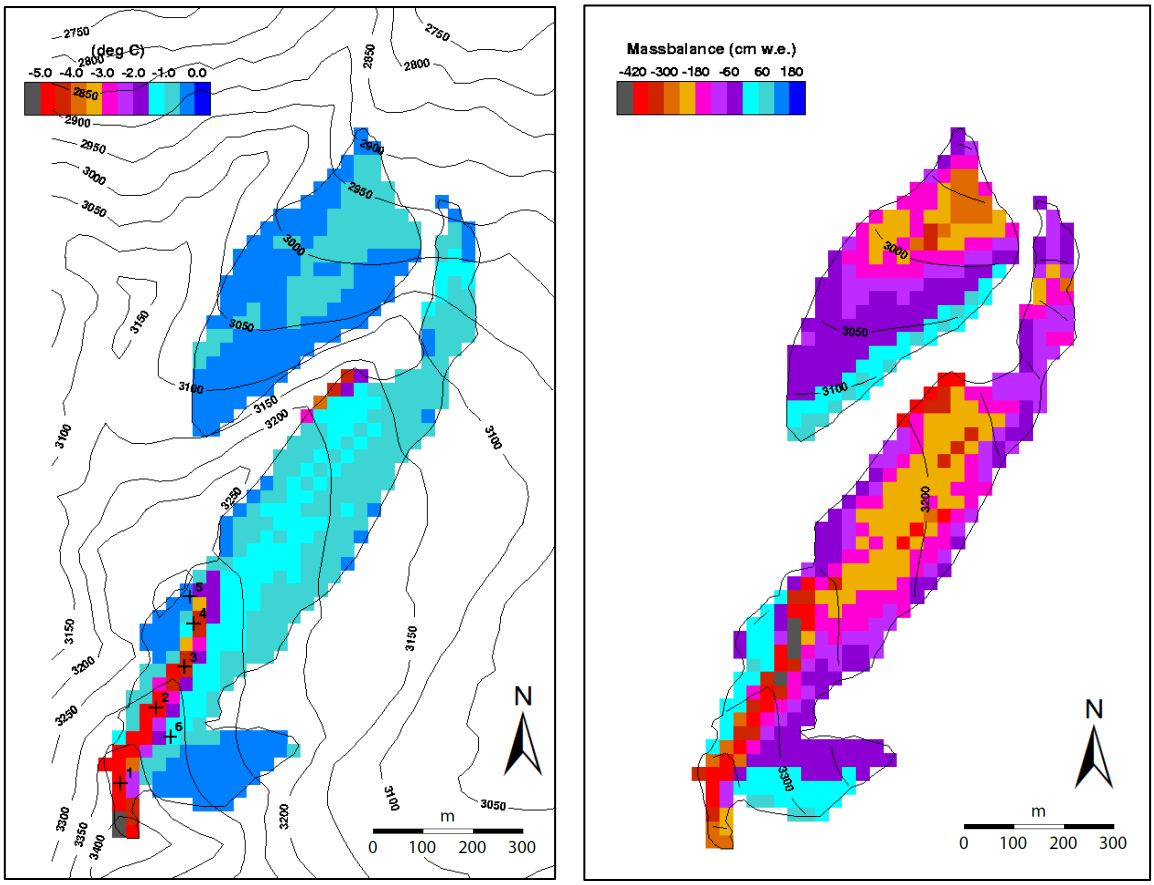

Figure 5.4: **(a)** Modelled minimum ice temperatures for the year 2000 for Vadret dal Corvatsch. The colours show lowest temperatures of an ice column. Lowest ice temperatures were modelled for the ice crest in the south-eastern part of the glacier. **(b)** Modelled mass balance values for the year 2002 for Vadret dal Corvatsch. The area of highest ablation corresponds with the area of lowest temperatures.

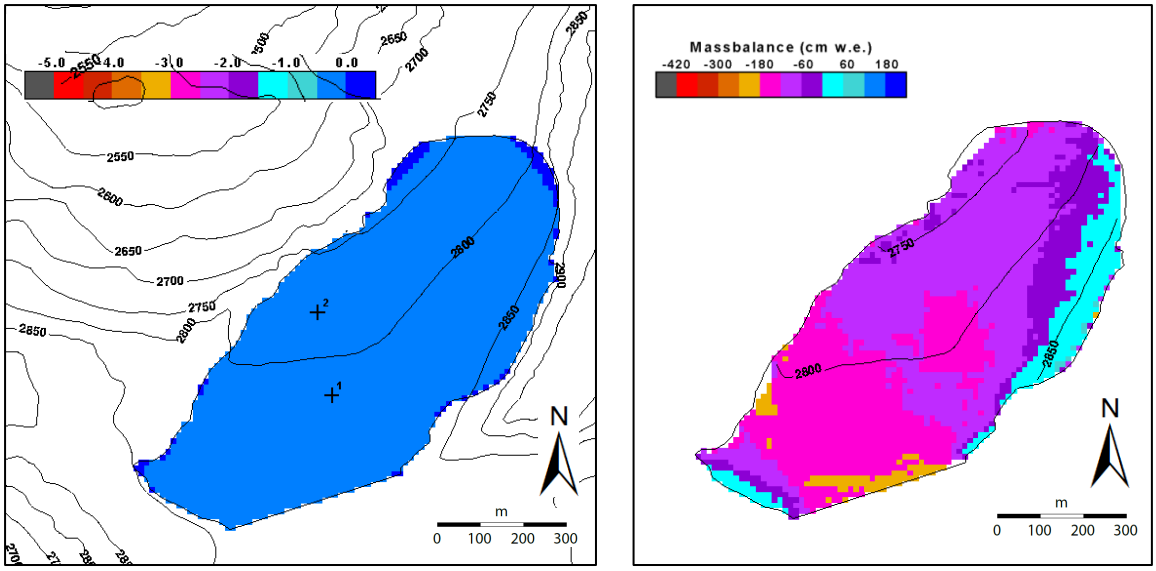

Figure 5.5: **(a)** Modelled minimum ice temperatures for the year 2010 for Glacier du Sex Rouge. The colours show lowest temperatures of an ice column. **(b)** Modelled mass balance values for the year 2013 for Glacier du Sex Rouge, showing accumulation at the very western part of the glacier and ablation at the rest of the glacier surface.

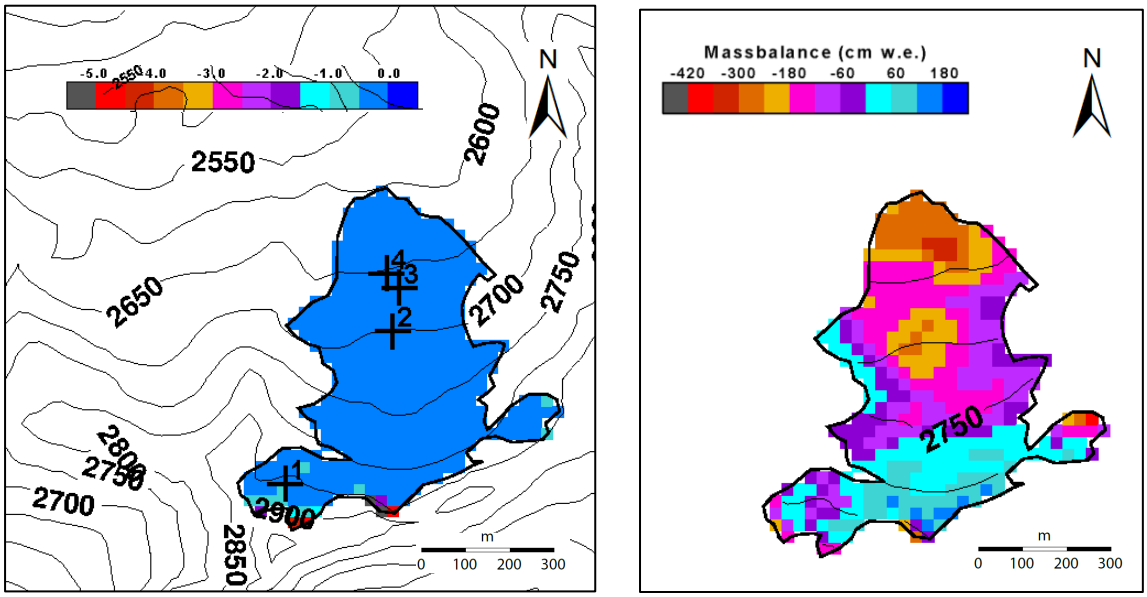

Figure 5.6: **(a)** Modelled minimum ice temperatures for the year 2010 for St. Annafirn. The colours show lowest temperatures of an ice column. **(b)** Modelled mass balance values for the year 2013 for St. Annafirn, showing accumulation at the upper part of the glacier and ablation at the middle part and the glacier tongue.

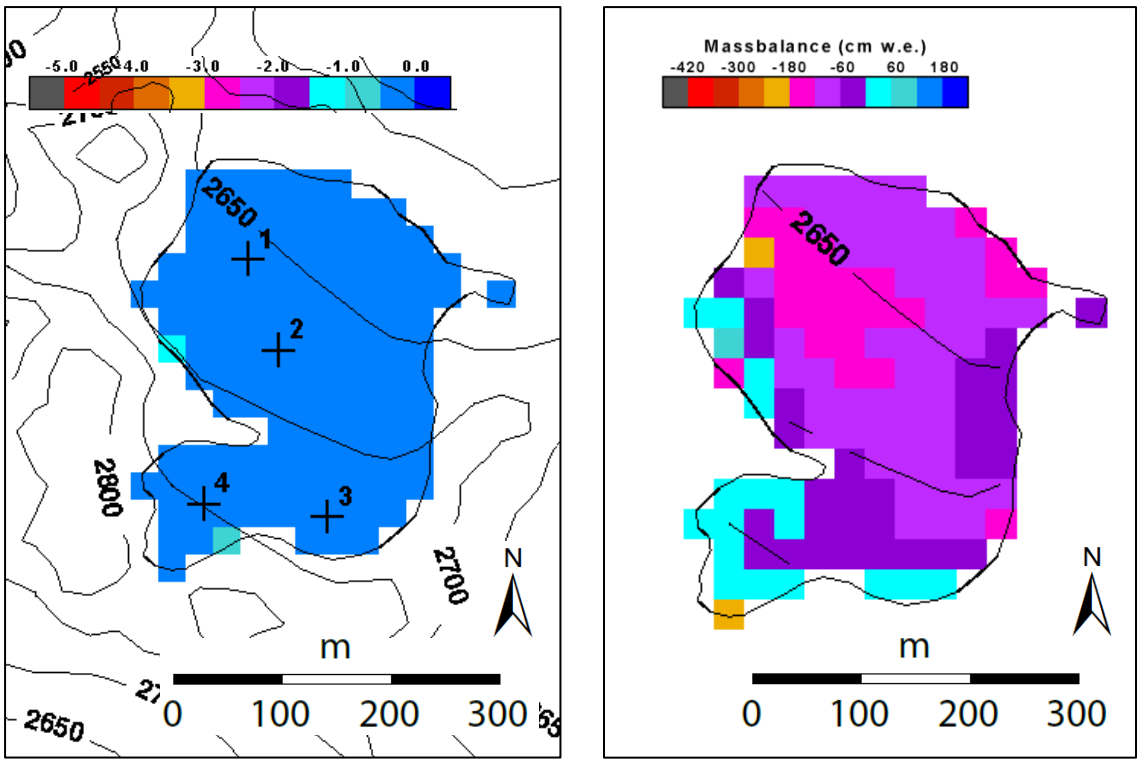

Figure 5.7: **(a)** Modelled minimum ice temperatures for the year 2010 for Pizolgletscher. The colours show lowest temperatures of an ice column. **(b)** Modelled mass balance values for the year 2013 for Pizolgletscher, showing accumulation at the upper part of the glacier and ablation at the rest of the glacier surface.

5.1.3. Temporal evolution of modelled ice temperatures

In Figure 5.8, an overview of modelled 10m-ice temperatures over time – including the application of different climate scenarios – is given. The red frame highlights a simultaneous temperature drop 0.35-0.45°C for all glaciers around the year 2005. The drop is especially noticeable at Glacier du Sex Rouge and Pizolgletscher since here modelled temperatures were rather stable since 1980.

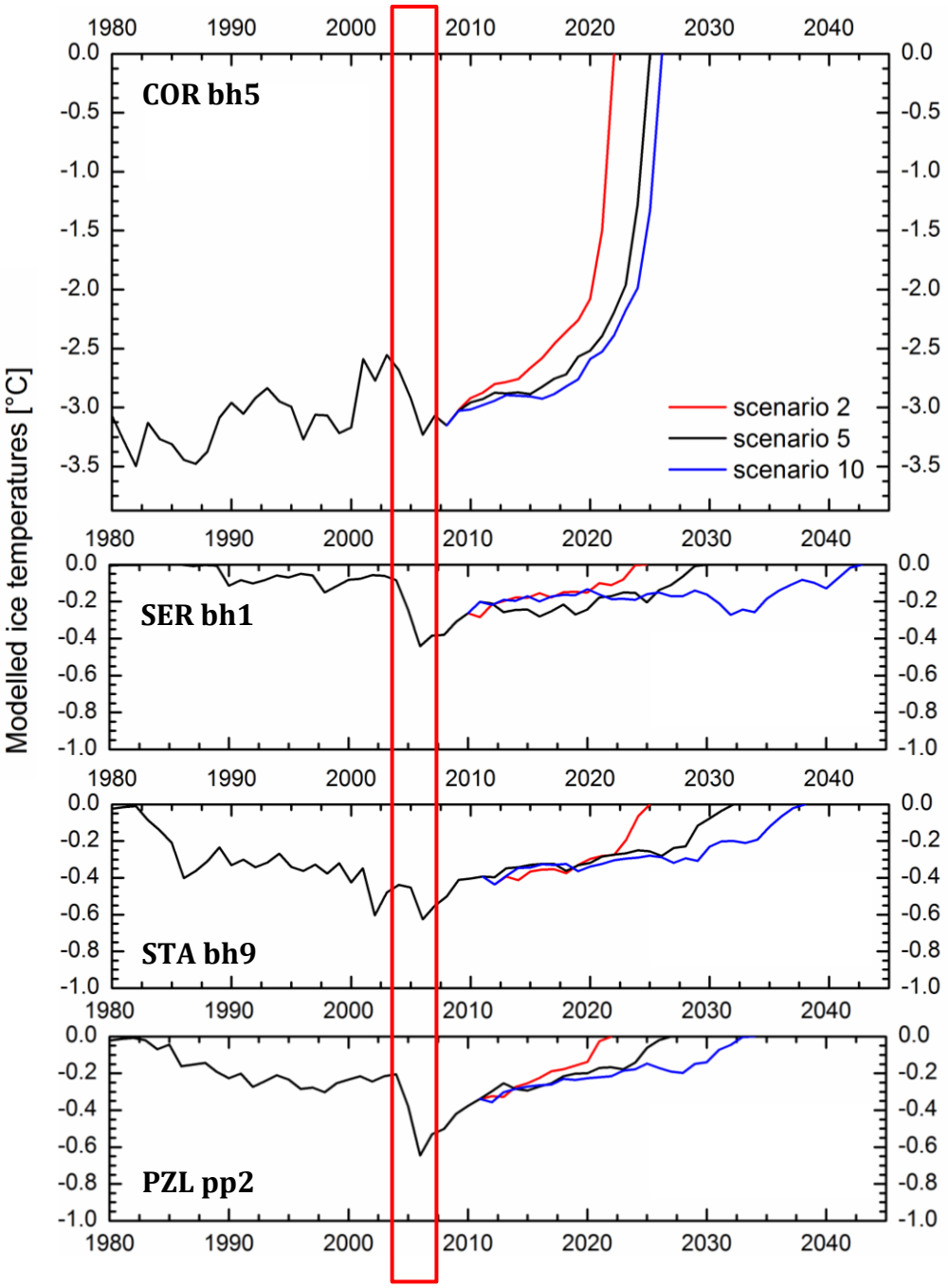

Figure 5.8: Modelled 10m-temperatures over time for Vadret dal Corvatsch (COR, borehole 5), Glacier du Sex Rouge (SER, borehole 1), St, Annafirn (STA, borehole 9) and Pizolgletscher (PZL, point 2), showing different future scenarios. The red frame highlights a simultaneous temperature drop for all glaciers. The year where the 10m-temperature reaches 0°C, the glacier thickness falls below 10 m at the given location.

For Glacier du Sex Rouge, St. Annafirn and Pizolgletscher, the temperature drop around 2005 represents the absolute minimum of modelled temperatures from 1980 to the disappearance of the glacier. After 2005, 10m-temperatures rise slowly. Temperatures at a depth of 20 m show a similar pattern. 20m-temperatures slowly decrease until about 2010, then starting to rise until the end of the glacier lifetime (Figure 5.10).

Vadret dal Corvatsch doesn't show any comparable decreasing temperatures at a depth of 20 m. Here, temperatures fall by 0.11°C between 2005 and 2010. Vadret dal Corvatsch is located at higher elevation than the other three glaciers and the MAAT is therefore lower. It is possible that no disappearance of the firn layer is modelled and thus no significant lowering of ice temperatures is displayed.

The difference of modelled ice temperatures predicting meltwater at the glacier base or without predicting meltwater is nicely seen in Figure 5.9. If the temperature at the glacier bed is set to 0°C, it also affects temperatures at shallower depths. The thinner the glacier gets, the higher 10m-temperatures result. When the glacier thickness falls below 10 m, the 10m-temperature reaches 0°C.

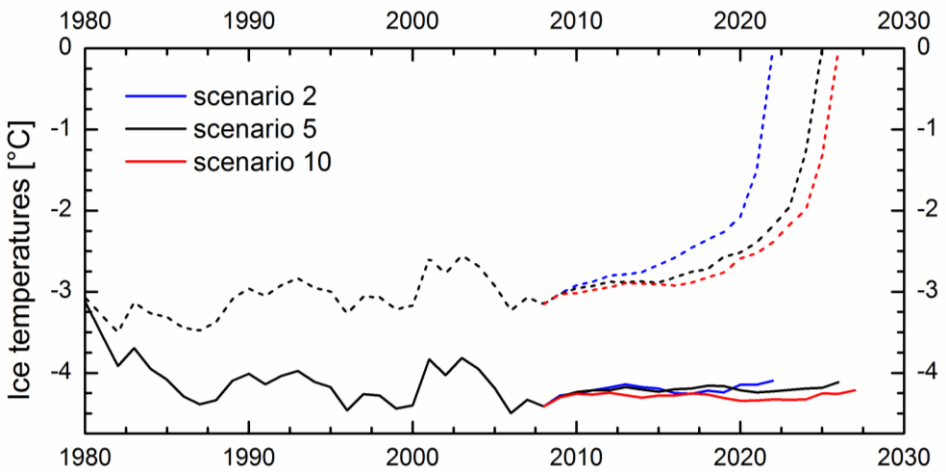

Figure 5.9: Comparison of modelled 10m-temperatures over time for borehole 5 at Vadret dal Corvatsch. The dashed lines indicate scenarios predicting meltwater at the glacier base, solid lines indicate scenarios without assuming meltwater at the glacier base.

The temporal evolution of ice temperatures is especially interesting at depths where seasonal temperature fluctuations vanish. For Glacier du Sex Rouge, St. Annafirn and Pizolgletscher, temperatures in the depth of 20 m were modelled temperate in the 1980s. 20m-temperatures then slowly decreased for those glaciers, exhibiting a major drop beginning in 2005. Near the end of the modelled future lifetime of the individual glaciers, 20m-temperatures rise to 0°C.

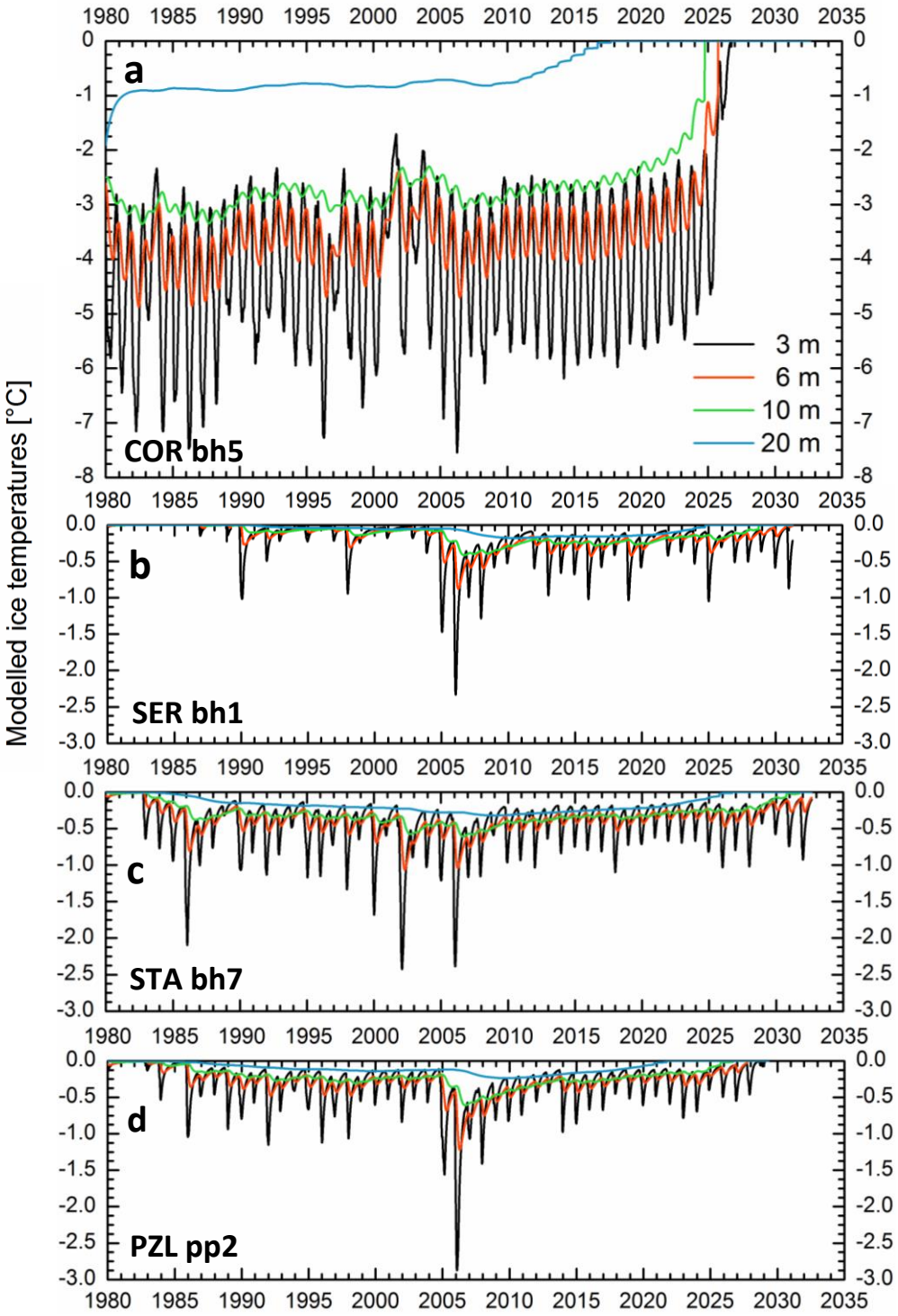

Figure 5.10: Modelled ice temperatures of **(a)** borehole 5 at Vadret dal Corvatsch, **(b)** borehole 1 at Glacier du Sex Rouge, **(c)** borehole 7 at St. Annafirn, and **(d)** point 2 at Pizolgletscher at different depths over time. All ice temperatures were modelled predicting meltwater at the glacier base.

5.2. CTS determined from radar data

The analysed GPR profiles partly show a distinct change in the density of backscatter. At Vadret dal Corvatsch, Glacier du Sex Rouge and St. Annafirn, spatial information of a GPR could be included and thus the spatial distribution of borders of different water content could be generated. For Pizolgletscher, qualitative data was included as no GPS data was available.

5.2.1. Vadret dal Corvatsch

For Vadret dal Corvatsch, a similar task was already carried out by Busarello in 2002. He found that the RTS was located within the cold ice zone that was defined by Hager (2002). Here, the analysed GPR profiles of the year 2013 showed no distinct RTS, therefore only a qualitative analysis was carried out. At profiles of the upper part of the glacier and particularly of the ice crest, the bed was generally clearly visible, whereas profiles located at the lower part of the glacier rather showed some denser backscatter.

5.2.2. Glacier du Sex Rouge

At 10 GPR profiles of Glacier du Sex Rouge in 2012, a distinct zone of denser backscatter is visible. All retrieved information about the depth of the radar transition zone (RTS) is represented in Figure 5.11. Greater depths of the RTS emerged at the middle and towards the western part of the glacier, while lower depths are present at the eastern part of the glacier. One GPR profile near each borehole is provided in Figure 5.12 andFigure 5.13. The point of nearest distance to the individual borehole is indicated by a yellow line within the profile.

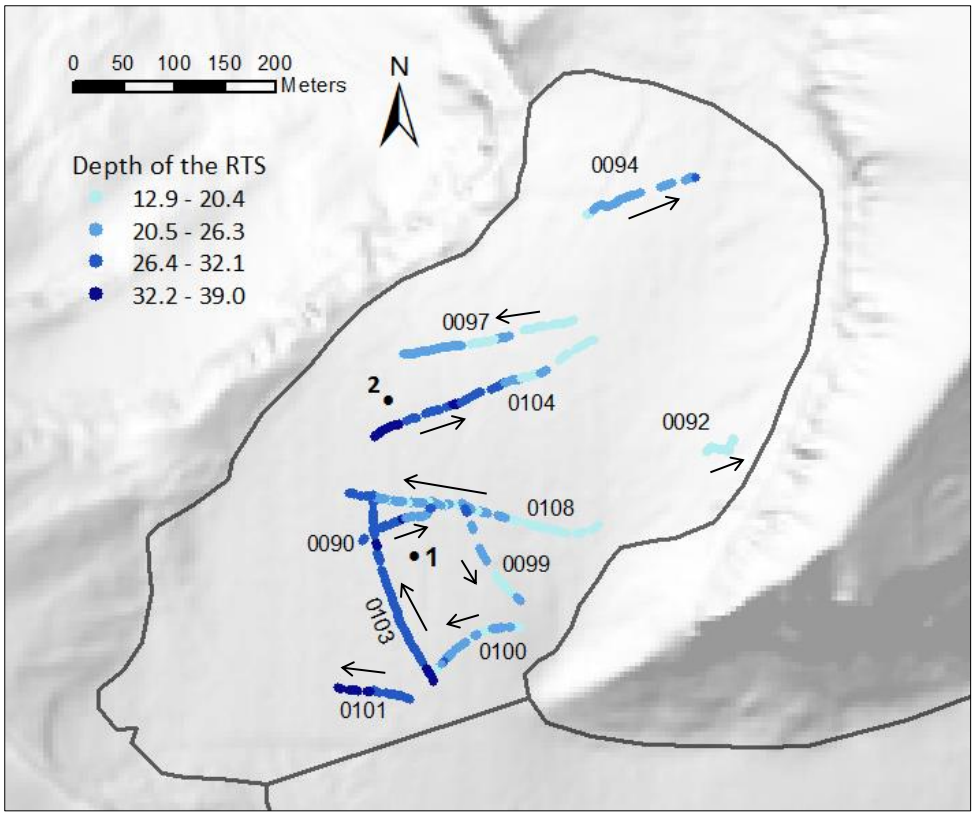

Figure 5.11: Depths of the RTS at Glacier du Sex Rouge. Depth values are retrieved from 10 selected GPR profiles carried out by Mauro Fischer in 2012. The arrows show the direction of travel during the acquisition of the profiles. The locations of the two boreholes are indicated by black dots.

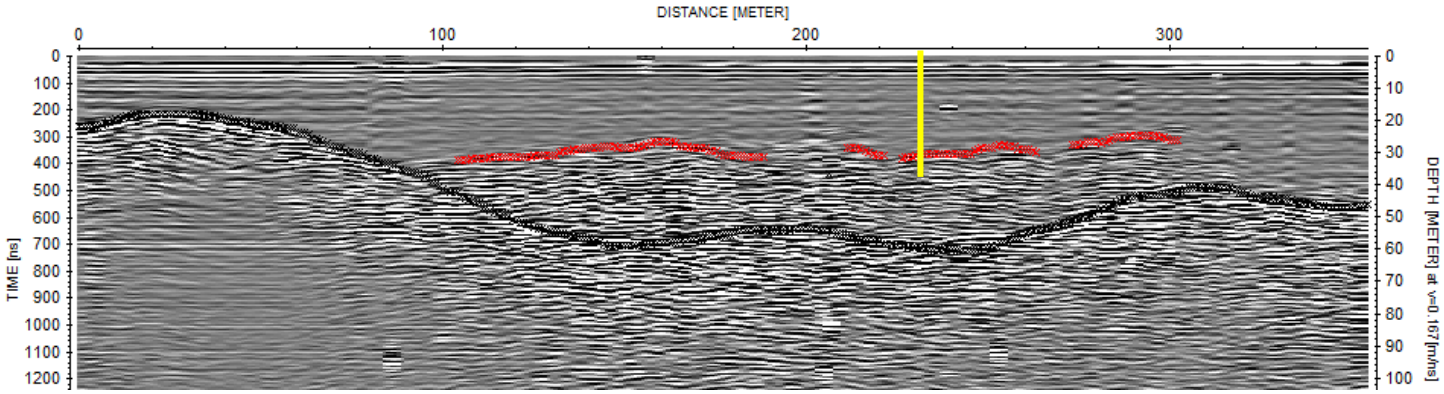

Figure 5.12: GPR profile 0103 of Glacier du Sex Rouge, carried out in 2012 by Mauro Fischer. The yellow line indicates the closest distance (about 36 m) to borehole 1.

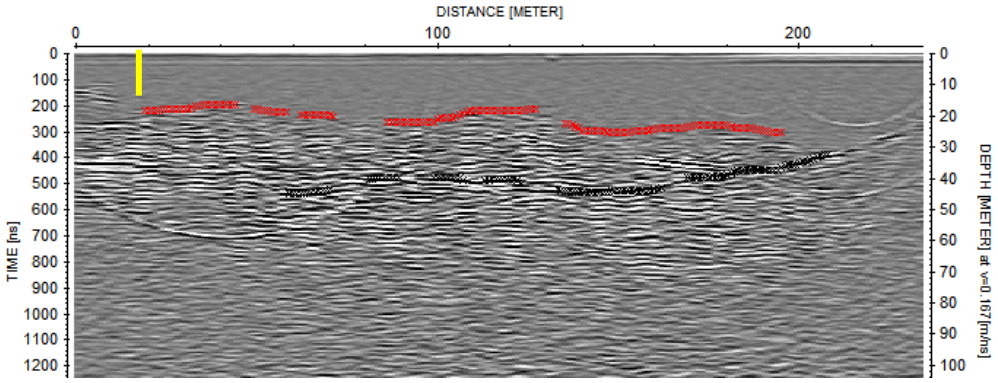

Figure 5.13: GPR profile 0097 of Glacier du Sex Rouge, carried out in 2012 by Mauro Fischer. The yellow line indicates the closest distance (about 42 m) to borehole 2.

5.2.3. St. Annafirn

At St. Annafirn, 5 profiles of the year 2013 show a nicely visible RTS. These profiles were all carried out at the main middle part of the glacier. In the nearest available profile to borehole 9, no distinct RTS can be constituted (Figure 5.15). The closest GPR profile showing a distinct RTS can be seen in Figure 5.16.

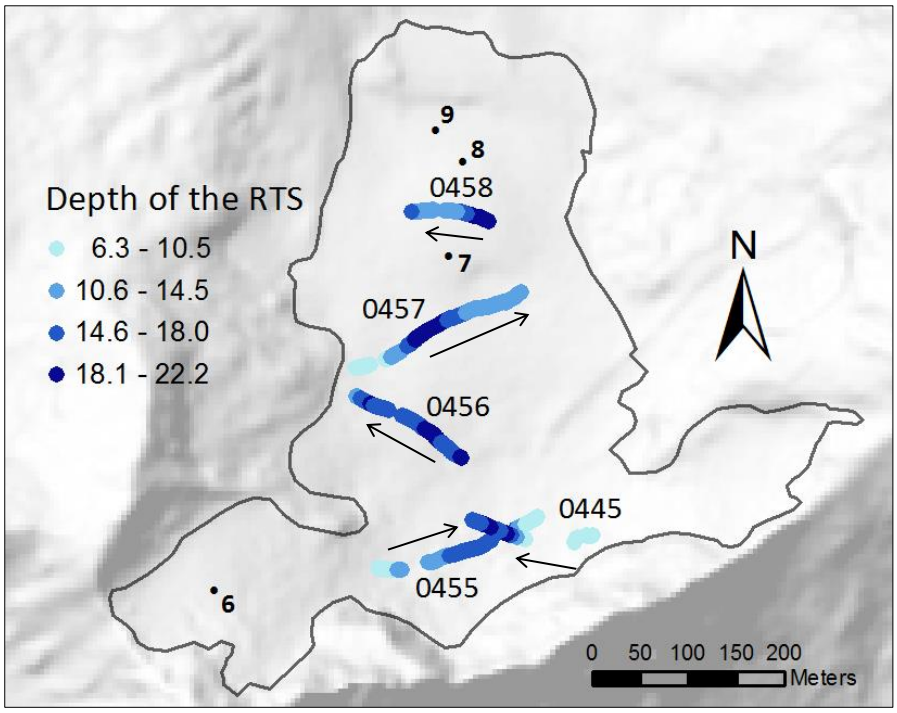

Figure 5.14: Depths the RTS at St. Annafirn. Depth values are retrieved from 5 selected GPR profiles carried out by Mauro Fischer in 2013. The arrows show the direction of travel during the acquisition of the profiles. The locations of the two boreholes are indicated by black dots.

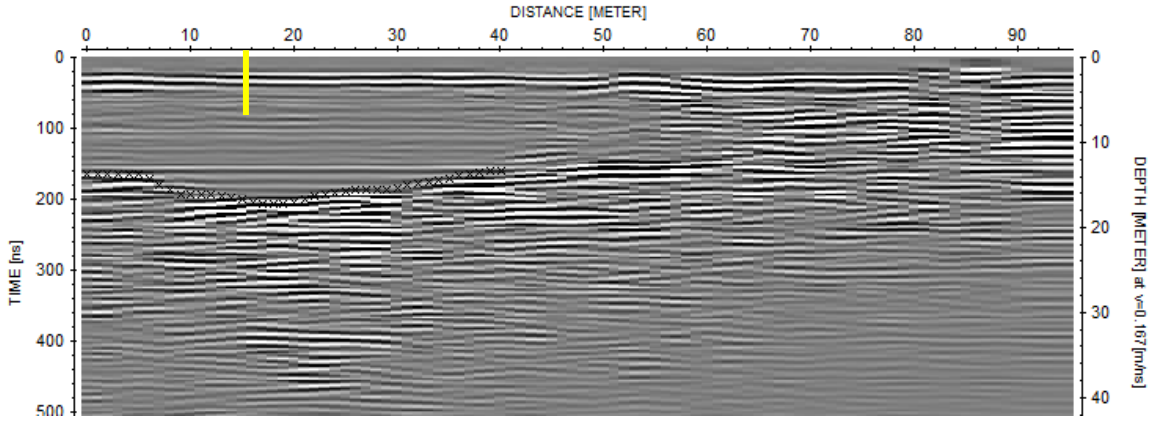

Figure 5.15: GPR profile 0461 of the tongue of St. Annafirn, carried out in 2013 by Mauro Fischer. The profile is parallel to profile 0458 (Figure 5.14). The yellow line indicates the closest distance (about 17 m) to borehole 9. As no distinct RTS is visible on this profile, it was not included in Figure 5.14.

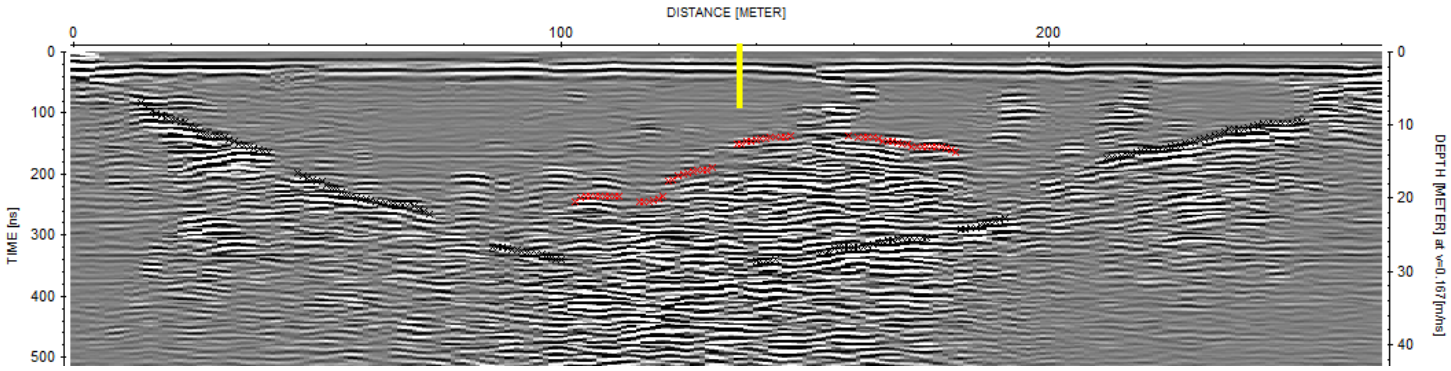

Figure 5.16: GPR profile 0458 of St. Annafirn, carried out in 2013 by Mauro Fischer. The yellow line indicates the closest distance (about 46 m) to borehole 7 (for which no temperature measurements are available). The distance to borehole 9 is about 82 m.

In the western little basin of St. Annafirn, most profiles don't show a distinct RTS. At two GPR profiles, denser backscatter is visible at the upper part of the glacier (red circle in Figure 5.17). Since the backscatters of these zones were interpreted to originate from debris, those profiles were not included in the overview of the RTS provided in Figure 5.14. The closest profile to borehole 6 is given in Figure 5.18. The point of nearest distance to the individual borehole is indicated by a yellow line within the profile.

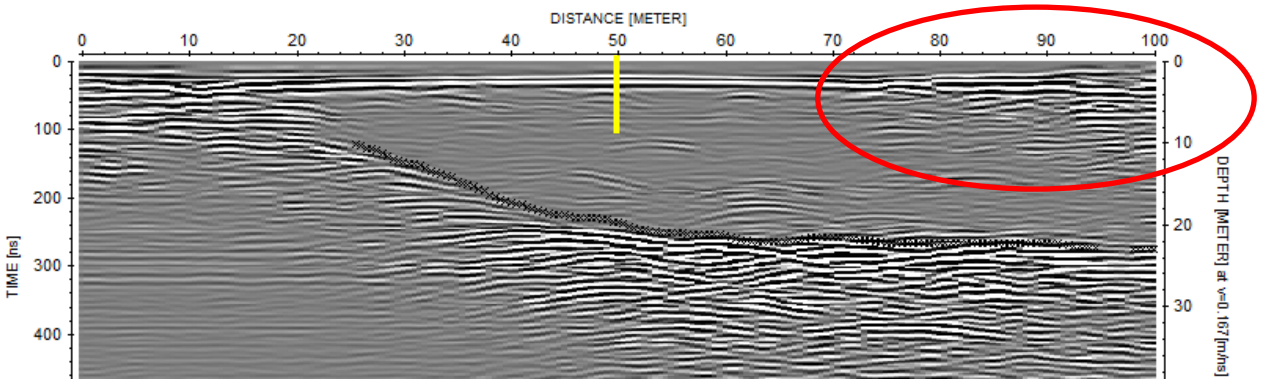

Figure 5.17: GPR profile 0452 of the western little basin of St. Annafirn, carried out in 2013 by Mauro Fischer. The yellow line indicates the closest distance (about 65 m) to borehole 6. As no typical RTS is visible on this profile, it was not included in Figure 5.14.

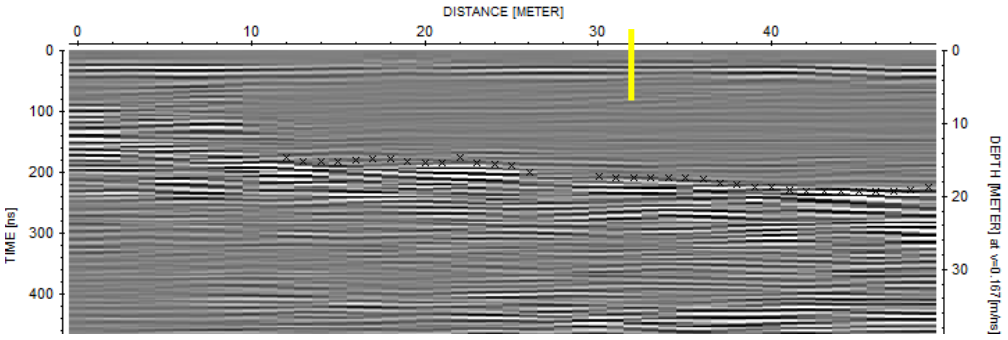

Figure 5.18: GPR profile 0450 of St. Annafirn, carried out in 2013 by Mauro Fischer. The yellow line indicates the closest distance (about 18 m) to borehole 6. As no distinct RTS is visible on this profile, it was not included in Figure 5.14.

5.2.4. Pizolgletscher

As no GPR data was available, a qualitative assessment was carried out. Several profiles show a very clear change in backscatter pattern at a depth of 20±5 m (Figure 5.19).

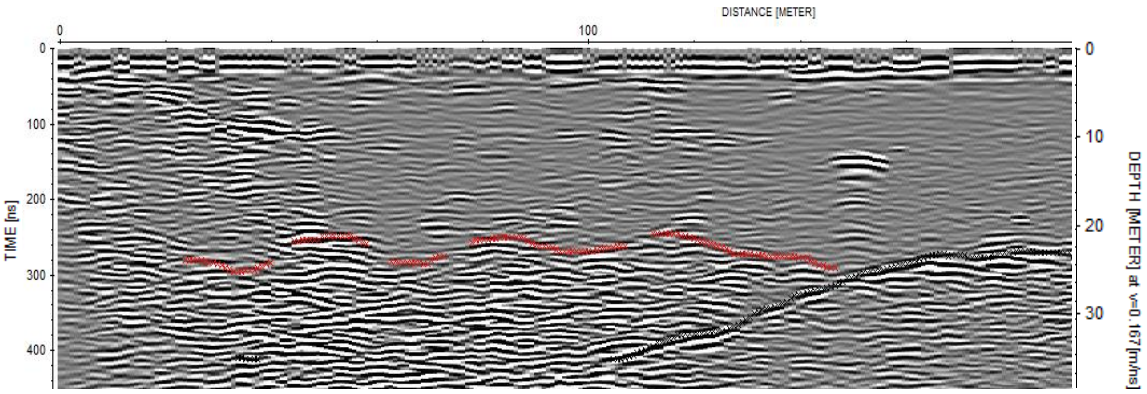

Figure 5.19: GPR profile 0104 of Pizolgletscher carried out by Matthias Huss in 2010 nicely shows the glacier bed (black) and a distinct zone of more backscatter starting at a depth of about 20 m (red).

5.2.5. Accuracy

The accuracy of the RTS is determined by two factors; the accuracy of the radar profile itself and the accuracy of the picking. In other studies, the uncertainty of GPR profiles were assumed to be ±1 m (Pettersson *et al.* 2003), or ±2-3 m (Fischer 2009). As here GPR is applied to detect RTS in depth of 20-30 m, the accuracy was estimated to be ±1 m. Picking accuracy was assumed to be ±5 m. Thus, an overall accuracy of ±6 m results.

There is an uncertainty in detecting the CTS from GPR profiles in general. Denser backscatter might result from other sources than liquid water, as e.g. debris or other impurities within the ice (Eisen *et al.* 2009).

6. Discussion

First of all, the modelled ice temperatures and the performance of the applied model will be discussed. Then, further information retrieved by the GPR profiles is gathered and finally, all available data is combined for the interpretation of measured borehole temperatures.

6.1. Modelled ice temperatures with GERM

Modelled temperatures are a result of the following variables:

- Input air temperatures
- Snowcover height (insulation)
- Glacier thickness (if water is simulated at the glacier bed, see Figure 6.2)
- Amount of meltwater stored within the firn pack

The model outputs show temperatures below the PMP for major parts of all four modelled glaciers. By far the lowest temperatures were modelled for Vadret dal Corvatsch, then for St. Annafirn and Pizolgletscher. Finally, for Glacier du Sex Rouge highest values were modelled. This order agrees with the measured englacial temperatures. Comparison of different boreholes located at the same glacier show some lesser agreement. Differences of up to 0.9°C were calculated at Glacier du Sex Rouge and St. Annafirn, for Vadret dal Corvatsch the uncertainties are even higher (Table 5.1). The lack of further temperature measurements makes it difficult to assess the uncertainty of the model.

6.1.1. Penetration of the winter cold into the glacier ice

It takes some time for the low winter surface temperatures to get transmitted into the glacier ice by thermal conduction. The comparison between measured and modelled ice temperatures at different dates of the year showed, that the annual amplitude of the englacial temperatures is represented correctly in the model, but the range of the amplitude is not high enough. The underrepresentation of the annual cycle leads to less extreme temperature values near the surface. Near-surface temperatures should thus be handled with care. Modelled 10m-temperatures only show annual amplitude of less than 0.2°C; modelled temperatures at a depth of 20 m show no annual cycle at all anymore. Temperatures as this depth only react slowly; for the 20m-temperatures, it takes about 5 years to adjust to a major temperature change at the surface – what can be nicely seen at

Glacier du Sex Rouge in the years 2005-2010 (Figure 5.10b). As no such deep temperature measurements are available over time for the interrogated glaciers, no validation of the temporal evolution at such depths can be carried out. Because of the long reaction time, the lower ice temperatures in 2005 are very likely a result of surface temperatures about two seasons back. The heat summer 2003 melted away the firn cover of the very small glaciers, removing the possibility the meltwater storage at the surface. Thus, no latent heat could be released due to refreezing of meltwater in the cold firn pack (Gilbert *et al.* 2012). Figure 6.1 shows that also Tête Rousse Glacier in the Mont Blanc area exhibits lower 20m-temperatures as in 1980.

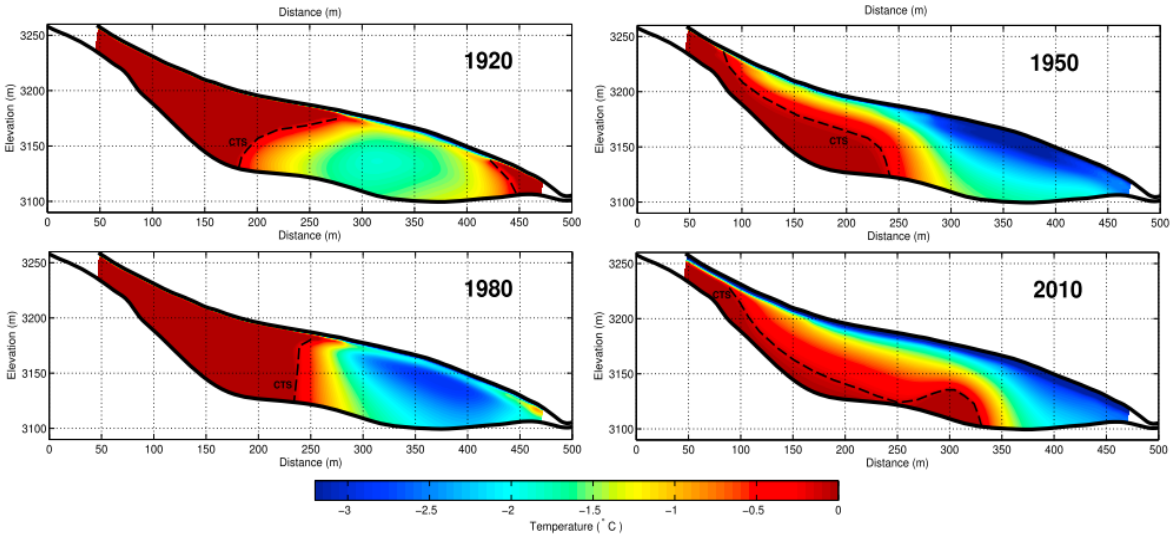

Figure 6.1: Evolution of ice temperatures at Tête Rousse Glacier for six different dates over the last 100 years, published in Gilbert *et al.* (2012).

The reason why the decrease of the modelled 20m-temperature of Vadret dal Corvatsch is smaller than at the other three glaciers might be, that the MAAT are lower and thus no disappearance of the firn layer is modelled.

6.1.2. Influence of glacier bed hydrology

Modelled temperatures at greater depths nicely show the difference between the scenario assuming meltwater and assuming no meltwater at the glacier base (e.g. Figure 5.2b). If meltwater at the glacier base is assumed, 0°C is set at the glacier base, which leads to higher modelled temperatures throughout the glacier because of heat conduction.

At Glacier du Sex Rouge, measurements at the thickest part of the glacier showed that the glacier is at the PMP below the depth of 22-25 meters. Figure 5.1 shows that the scenario predicting meltwater at the glacier base results in a better representation of the actual ice temperatures than the scenario assuming no meltwater at the glacier base. Still, modelled ice temperatures for the upper part of the glacier are too high, while the lower part of the glacier is modelled slightly too warm.

As all of the available temperature measurements of Vadret dal Corvatsch and St. Annafirn are of the upper 15 or even 10 meters, no validation of temperatures of greater depths could take place. Therefore no knowledge of the situation near the bed is available. This would be important to know whether to dictate meltwater at the glacier base or not.

In view of the disappearance of glaciers in the future, the assumption of meltwater at the glacier base is reasonable. If no meltwater is predicted at the base, the modelled glaciers vanish without ever experiencing temperatures near the melting point. For example at Vadret dal Corvatsch, modelled ice temperatures are still around -4°C for the year the glacier is assumed to disappear (Figure 5.9). If meltwater is simulated at the glacier base, ice temperatures are affected by the decreasing glacier thickness. Temperatures rise fast when the thickness of the glacier at the given location gets closer to the depth at which the modelled temperatures are plotted. If for example the glacier thickness approaches 10 m, the 10m-temperature reaches 0°C. At the time the glacier disappears, the remaining ice is temperate.

It is not yet possible to simulate meltwater at specified depths or locations. If knowledge about the occurrence of water bodies within the glacier could be implemented in the model, the model performance could be improved. Information about the glacier hydrology could be retrieved by GPR as it has been carried out for Glacier du Sex Rouge, St. Annafirn and Pizolgletscher. However, the future situation of the glacier hydrology remains unclear.

6.1.3. Limitations of the applied model

GERM was originally designed to model mass balance and runoff of bigger (valley) glaciers in the Swiss Alps. To obtain reasonable mass balance values for very small glaciers, the implemented algorithms should be tuned to predominant mechanisms at those glaciers. The main improvement of adjusted mass balance calculations is the survival time of the glaciers and glacier thickness. Realistic thickness values are mainly important if meltwater at the glacier base is dictated. If for example the future glacier thickness is modelled 10 m instead of 20 m, a steeper temperature from the surface to the supposed bed results; as shown in Figure 6.2. Thus, temperatures of the whole glacier are affected.

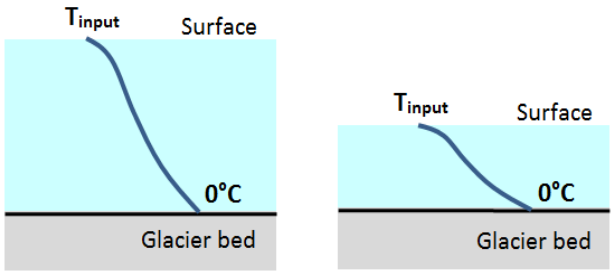

Figure 6.2: Schematic illustration of the influence of glacier thickness if meltwater is dictated at the glacier base.

A minor issue of the model is the fact, that ice temperatures have no influence on the mass balance and thus for the future lifetime of the modelled glaciers. In the applied energy balance model according to Oerlemans (2001), all glacier ice is assumed to me at the melting point. However a part of the input energy is needed to first heat up the glacier to the PMP before any melting takes place. Since it takes only 2% more energy to heat ice of -2°C up to the melting point than it takes to melt the ice, lower temperatures won't affect the glacier mass balance significantly. Yet, decreasing temperatures might influence the mass balance of a glacier due to a different glacier hydrology. If cold ice exists at the glacier base, the glacier is frozen to its bed; resulting in a very limited ice motion. Yet, also this influence is assumed to be minor, since very small glaciers are rather stable anyways.

A further slight issue for very small glacier is the fact, that the PMP is not implemented in the model; Temperatures of 0°C is possible at any depth. As the modelled very small glaciers show maximum depths of about 60 m, the PMP doesn't fall below -0.05°C; resulting in only small errors.

6.1.4. Input data evaluation

The meteorological input data are not of the same quality for all interrogated glaciers. While for Vadret dal Corvatsch a weather station is located right beside the glacier, input meteo data for Pizolgletscher, for example, is retrieved from a station located at a distance of 32 km from the glacier. As the air temperature is one of the main drivers of the modelled ice temperatures, it is important that a good input data quality is given. Nevertheless it is questionable if improved input temperature values cause a significant improvement of the temperature model performance.

The input DEM and glacier outlines are of lower importance for the modelled ice temperatures. They mainly have influence on the glacier thickness and will mainly have an influence if meltwater is dictated at the glacier bed.

6.1.5. Conceptual validation

The model assumes that glacier ice is fully impermeable for water. However it is possible for meltwater to reach the interior of a cold glacier by englacial passages formed by meltwater channels or by moulins that develop on a seasonal basis (Bælum and Benn 2011). Such features are not implemented in the model. Furthermore, melt is possible up to a depth of about a meter due to radiation that enters the upper brittle part of the glacier ice.

Since GERM models ice temperatures at the right order of magnitude for all glaciers where measurements are available and a decrease of 20m-temperatures is visible in the modelled data, it can be assumed that the most important processes influencing ice temperatures of very small glaciers are implemented in the model.

The model is only suitable for glaciers where some knowledge about the glacier hydrology is available. Heat advection and the influence of penetrating meltwater into crevasses is not implemented in the model, thus only glacier with low vertical flow are suitable for the model.

6.2. CTS determined from radar profiles

The RTS most certainly accounts for free water present in the glacier as it was already suggested in earlier studies (e.g. Pettersson 2004, Gusmeroli *et al.* 2010, Bælum and Benn 2011). Pettersson *et al.* (2003) found some good agreement of the RTS and the CTS for Storglaciären in Sweden, whereas Eisen *et al.* (2009) found major differences between the two at the tongue of Gornergletscher in the Valais (Switzerland).

Both Glacier du Sex Rouge and St. Annafirn show greater depths of the zone of denser backscatter in the middle of the glacier. Therefore the assumption that the RTS originates from debris is rejected. Henceforth, the zone of higher backscatter intensity is referred to as the water-saturated layer. In general, lowest temperatures were measured at locations where no water-saturated zone could be defined. Thus, these zones were interpreted as being cold.

6.2.1. Hydrology of Glacier du Sex Rouge

At the western part of Glacier du Sex Rouge, the saturated zone starts at greater depths (27-35 m) than in the eastern part (17-20 m). A possible explanation for this phenomenon can be seen in the accumulation pattern of the glacier. Additional accumulation is gained by avalanches coming from the Oldenhorn (located in the east of the glacier). Thus, more meltwater is produced within the resulting larger snowpack.

Near borehole 1 at Glacier du Sex Rouge, the water-saturated layer starts at a depth of 27±6 m in 2012 and thus accounted for almost half of the glacier thickness. In the hydrological year 2013 (1st October 2012-30th September 2013), ablation of 0.4 m was measured near borehole 1. This value has to be subtracted from the depth of the water-saturated layer in order to compare this depth to the CTS retrieved from borehole temperature measurements a year later. Borehole temperature measurements in 2013 and 2014 showed, that the CTS changes over time as well. A decrease of around 1±0.5 m was estimated for the mentioned period (Figure 3.1b). Thus, the uncertainty of the depth of the water-saturated layer increases to 7.5 m a^{-1}.

For the year 2013, the upper limit of the saturated zone is about 4 m lower than the CTS retrieved by the borehole temperature measurements (22-23 m) and is thus still in the range of uncertainty. Unfortunately no measurements of the CTS for other boreholes are available for further comparisons.

However the measured CTS might be higher than the RTS, since the CTS refers to a change in temperature, while the RTS results from a change in water content. It is possible, that an unsaturated temperate ice exists above the saturated layer and is thus not visible on GPR profiles. On the other hand, the RTS might also be caused by local water pockets or backscatter from an irregular CTS (Eisen *et al.* 2009).

If the border to the water-saturated zone really indicates the CTS, it makes sense that the water-saturated zone starts at greater depth at borehole 2, as here lower temperatures were measured than for borehole 1. Temperatures at the eastern part of the glacier are assumed to be higher, as the cold surface layer is thinner; probably because of the enhanced meltwater production.

6.2.2. Hydrology of St. Annafirn

At the main middle part of St. Annafirn, a saturated zone is withdrawn from the GPR profiles, starting at about 15-20 m below the glacier surface. Towards the western glacier margin as well as the southern top of the glacier, the saturated zone starts already at depth of 7-10 m. The nearest GPR profiles of borehole 9 don't show any zone of denser backscatter (therefore not included in Figure 5.14), leading to the conclusion that no saturated zone is present at the lowest part of the glacier. It is likewise possible that the glacier contains cold ice down to the bed.

A different pattern is prevailed at the western little basin (lower left corner in Figure 5.14). Here, denser backscatter is visible just below the surface in two profiles. This zone is between 6 and 8 m thick and only some tens of meters wide. The rest of the profiles show no RTS and a clearly visible bed. As at borehole 6 negative temperatures (-1.27°C) were measured in a depth of 7.24 m. It is not likely that the denser backscatter originates from meltwater within the upper part of the cold ice, as no crevasses are present at the basin. Due to the location near a rockwall and the limited extent of the backscatter zone, it might originate from debris fallen onto the glacier in earlier years.

6.2.3. Assumptions for Pizolgletscher

At Pizolgletscher, some GPR profiles very nicely show the presence of meltwater below a depth of 20 m (Figure 5.19). Since the change in the backscatter density is rather abrupt and modelled ice temperatures are even below the ones of St. Annafirn, it can be assumed that the border also accounts for the CTS and the glacier is cold at its upper part. As no temperature field data is available for Pizolgletscher, this assumption can't be confirmed.

6.3. Interpretation of measured ice temperatures

6.3.1. Glacier du Sex Rouge

At borehole 1 at the thickest part of Glacier du Sex Rouge, cold ice is present at the upper 20-25 m of the glacier. At a depth of 20 m, no major seasonal changing occurs. It can thus be concluded, that a zone of cold ice exists throughout the year. At borehole 2 – which lies at lower elevation and at a location of lower glacier thickness than borehole 1 – a surprisingly lower ice temperature was measured in September 2014 (Figure 5.1a). A reason for higher temperature at borehole 1 could be found in the time the locations usually get free of firn. If borehole 2 is free of firn for a longer period, less warming due to refreezing in the cold firnpack occurs (Gilbert *et al.* 2012). As the analysis of GPR profiles showed, more water is present at the eastern part of the glacier, giving evidence for a thicker temperate layer there as well.

A possible explanation for the temperate basal layer is the remnant of conditions from the time, where glaciers were still covered with firn, remained. Glacier ice at a depth of 25 m and below was built up under temperate conditions. After the disappearance of the firn cover, the winter cold now easily enters the glacier, leading to slow cooling from above. This approach suggest, that ice temperatures at very small glaciers still decrease.

6.3.2. St. Annafirn

At St. Annafirn, ice temperatures of -1.27°C and -0.29°C, respectively, were measured at borehole 6 and 9 in a depth of around 8 m. The lower value was measured at borehole 6 located at the south-western little basin with a depth of approximately 30 m. The elevation difference between the two boreholes is about 230 m and can't be the only reason for the difference in ice temperatures. Observations in the past two years showed, that around borehole 6 a circular patch of bare ice existed; indicating a small zone of ablation within the accumulation area (M. Fischer 2014, personal communication). This could be the result of snow redistribution processes. Although such a short observation period is not representative, it might indicate the reason for the observed ice temperature difference. The absence of a firn layer allows cold temperatures to easily enter the glacier ice at the western little basin. If the observed mass balance pattern repeats over several years, cold ice might be expected at locations, were ablation is high enough to melt the firn layer.

7. Conclusions

Ice temperatures of Vadret dal Corvatsch, Glacier du Sex Rouge, St. Annafirn and Pizolgletscher were modelled using an adapted version of GERM. Furthermore, GPR profiles of Glacier du Sex Rouge, St. Annafirn and Pizolgletscher were analysed in view of the detection of a cold-transition surface. The obtained results were then compared to measured borehole temperatures and used to answer the set research questions:

1. **Do very small glaciers in the Swiss Alps contain cold ice?**

It can be concluded, that very small glaciers in the Swiss Alps likely contain cold ice although they are situated at elevations below 3000 or even 2800 m a.s.l. The assumption of present cold ice within small glaciers is associated with the absence of major crevasses as well as extended firn areas covering the glacier.

2. **Is it possible to model ice temperatures of very small glaciers with an adapted version of GERM? Can the model be used to model future ice temperatures?**

The model is suitable to estimate whether the existence of cold ice within a very small glacier is possible. The evolution of temperatures at lower depths can be modelled, but not enough data at several dates is available for validation. Following tasks are not possible or should be carried out with care:

- Interpretation of the near surface temperatures; the amplitude of the annual cycle is modelled too low.
- Interpretation of spatial distribution of englacial temperatures for flat glaciers; temperatures of different boreholes at the same glacier were modelled too similar for Glacier du Sex Rouge.
- Detection of the CTS.

What could be further improved is the incorporation of saturated zones as present water leads to temperatures at the pressure melting point. With further information retrieved by the analysis of GPR profiles, such zones could be determined and included in the model.

The evolution of temperatures at greater depth should be validated by field data, as up to now, no such measurements are available.

3. Is it possible to detect cold ice within very small glaciers by means of GPR data?

It can't be concluded that the distinct change in backscatter density indicates the location of the CTS because not enough validation data is available. Only at the middle part of Glacier du Sex Rouge, a comparison of GPR data and CTS retrieved from borehole temperature measurements is possible, showing some good agreement.

The evidence of cold ice within very small glaciers contributes to the further process-understanding. At very small glaciers with no major crevasses, cold ice near the surface might be expected due to the melt of the firn cover. Ice at greater depths is assumed to be temperate at lower elevations, since it was probably built up under temperate conditions. Therefore, the use of very small glaciers as palaeo-climatic ice archives is questionable.

8. Literature

Bælum, K. and Benn, D.I., 2011. Thermal structure and drainage system of a small valley glacier (Tellbreen, Svalbard), investigated by ground penetrating radar. *The Cryosphere*, 5 (1), 139–149.

Bahr, D.B. and Radić, V., 2012. Significant contribution to total mass from very small glaciers. *The Cryosphere*, 6 (4), 763–770.

Bavay, M., Grünewald, T., and Lehning, M., 2013. Response of snow cover and runoff to climate change in high Alpine catchments of Eastern Switzerland. *Advances in Water Resources*, 55, 4–16.

Blatter, H. and Hutter, K., 1991. Polythermal conditions in Arctic glaciers. *Journal of Glaciology*, 37 (126), 261–269.

Bosshard, T., Kotlarski, S., Ewen, T., and Schär, C., 2011. Spectral representation of the annual cycle in the climate change signal. *Hydrology and Earth System Sciences*, 15 (9), 2777–2788.

Busarello, C., 2002. Sondierung des Gletscherbettes am Vadret dal Corvatsch mittels Georadar.

Chuece, J., Juliàn, A., and Lòpez-Moreno, J.I., 2007. Recent evolution (1981 – 2005) of the Maladeta glaciers, Pyrenees , Spain: extent and volume losses and their relation with climatic and topographic factors. *Journal of Glaciology*, 53 (183), 547–557.

Cuffey, K.M. and Paterson, W.S.B., 2010. *The physics of glaciers*. 4th ed. Academic Press.

DeBeer, C.M. and Sharp, M.J., 2009. Topographic influences on recent changes of very small glaciers in the Monashee Mountains, British Columbia, Canada. *Journal of Glaciology*, 55 (192), 691–700.

Eisen, O., Bauder, A., Lüthi, M., Riesen, P., and Funk, M., 2009. Deducing the thermal structure in the tongue of Gornergletscher, Switzerland, from radar surveys and borehole measurements. *Annals of Glaciology*, 50 (51), 63–70.

Farinotti, D., Usselmann, S., Huss, M., Bauder, A., and Funk, M., 2012. Runoff evolution in the Swiss Alps: projections for selected high-alpine catchments based on ENSEMBLES scenarios. *Hydrological Processes*, 26, 1909–1924.

Fischer, A., 2009. Calculation of glacier volume from sparse ice-thickness data, applied to Schaufelferner, Austria. *Journal of Glaciology*, 55 (191), 453–460.

Fischer, M., Huss, M., Barboux, C., and Hoelzle, M., 2014a. The new Swiss Glacier Inventory SGI2010: Relevance of using high-resolution source data in areas dominated by very small glaciers. *Arctic, Antarctic, and Alpine Research*, 46 (4), In press.

Fischer, M., Huss, M., and Hoelzle, M., 2014b. Surface elevation and mass changes of all Swiss glaciers 1980-2010. *The Cryosphere Discussions*, 8, 4581–4617.

Gellatly, A.F., Smiraglia, C., Grove, J.M., and Latham, R., 1994. Recent variations of Ghiacciaio del Calderone, Abruzzi, Italy. *Journal of Glaciology*, 40 (136), 486–490.

Gilbert, A., Vincent, C., Wagnon, P., Thibert, E., and Rabatel, A., 2012. The influence of snow cover thickness on the thermal regime of Tête Rousse Glacier (Mont Blanc range, 3200 m a.s.l.): Consequences for outburst flood hazards and glacier response to climate change. *Journal of Geophysical Research*, 117 (F4).

Goodrich, L.E., 1982. The influence of snow cover on the ground thermal regime. *Canadian Geotechnical Journal*, 19 (4), 421–432.

Gusmeroli, A., Murray, T., Jansson, P., Pettersson, R., Aschwanden, A., and Booth, A.D., 2010. Vertical distribution of water within the polythermal Storglaciären, Sweden. *Journal of Geophysical Research*, 115 (F04002), 1–14.

Haeberli, W., Frauenfelder, R., Kääb, A., and Wagner, S., 2004. Characteristics and potential climatic significance of "' miniature ice caps '" (crest- and cornice-type low-altitude ice archives). *Journal of Glaciology*, 50 (168), 129–136.

Hager, P., 2002. Glaziologische Untersuchungen am Gipfelgrat des Vadret dal Corvatsch: Thermik und Oberflächenprozesse. University of Zurich.

Hoelzle, M., 1994. Permafrost und Gletscher im Oberengadin. Grundlagen und Anwendungsbeispiele für automatisierte Schätzverfahren. *Mitteilung der Versuchsanstalt für Wasserbau, Hydrologie und Glaziologie (VAW) der ETH Zürich*, 132, 1–119.

Hooke, R.L., Gould, J.E., and Brzozowski, J., 1983. Near-surface temperatures near and below the equilibrium line on polar and subpolar glaciers. *Zeitschrift für Gletscherkunde und Glazialgeologie*, 19 (1), 1–25.

Hughes, P.D., 2007. Recent behaviour of the Debeli Namet glacier, Durmitor, Montenegro. *Earth Surface Processes and Landforms*, 32, 1593–1602.

Hughes, P.D., 2008. Response of a Montenegro glacier to extreme summer heatwaves in 2003 and 2007. *Geografiska Annaler, Series A, Physical Geography*, 90 (4), 259–267.

Hughes, P.D., 2009. Twenty-first Century Glaciers and Climate in the Prokletije Mountains, Albania. *Arctic, Antarctic, and Alpine Research*, 41 (4), 455–459.

Huss, M., 2010. Mass balance of Pizolgletscher. *Geographica Helvetica*, 65 (2), 80–91.

Huss, M., 2011. Present and future contribution of glacier storage change to runoff from macroscale drainage basins in Europe. *Water Resources Research*, 47 (7), W07511.

Huss, M., 2012. Extrapolating glacier mass balance to the mountain range scale: the European Alps 1900–2100. *The Cryosphere Discussions*, 6 (2), 1117–1156.

Huss, M., Bauder, a., Funk, M., and Hock, R., 2008a. Determination of the seasonal mass balance of four Alpine glaciers since 1865. *Journal of Geophysical Research*, 113 (F1), F01015.

Huss, M., Farinotti, D., Bauder, A., and Funk, M., 2008b. Modelling runoff from highly glacierized alpine drainage basins in a changing climate. *Hydrological Processes*, 22, 3888–3902.

Huss, M., Hock, R., Bauder, A., and Funk, M., 2010a. 100-year mass changes in the Swiss Alps linked to the Atlantic Multidecadal Oscillation. *Geophysical Research Letters*, 37 (10), L10501.

Huss, M., Hock, R., Bauder, A., and Funk, M., 2010b. 100-year mass changes in the Swiss Alps linked to the Atlantic Multidecadal Oscillation. *Geophysical Research Letters*, 37 (10), n/a–n/a.

Huss, M., Jouvet, G., Farinotti, D., and Bauder, A., 2010c. Future high-mountain hydrology: a new parameterization of glacier retreat. *Hydrology and Earth System Sciences*, 14 (5), 815–829.

Huss, M., Scherler, M., Schneider, S., Hoelzle, M., and Hauck, C., 2011. Future water yield from melting mountain permafrost : A fully distributed modelling approach. *Geophysical Research Abstracts*, 13 (EGU General Assembly 2011).

Huss, M., Zemp, M., Joerg, P.C., and Salzmann, N., 2014. High uncertainty in 21st century runoff projections from glacierized basins. *Journal of Hydrology*, 510, 35–48.

Hutter, K., Blatter, H., and Funk, M., 1988. A model computation of moisture content in polythermal glaciers. *Journal of Geophysical Research*, 93 (B10), 12205.

IPCC, 2013. *Climate Change 2013. The Physical Science Basis. Working Group I. Contribution to the Fifth Assessment Report of the Intergovernmental Panel on Climate Change*. WMO/UNEP, Cambridge University Press: WMO/UNEP, Cambridge University Press.

Jol, H.M. and Smith, D.G., 1991. Ground penetrating radar of northern lacustrine deltas. *Canadian Journal of Earth Sciences*, 28 (12), 1939–1947.

Kuhn, M., 1995. The mass balance of very small glaciers. *Zeitschrift für Gletscherkunde und Glazialgeologie*, 31, 171–179.

López-Moreno, J.I., Nogués-Bravo, D., Chueca-Cía, J., and Julián-Andrés, A., 2006. Glacier development and topographic context. *Earth Surface Processes and Landforms*, 31, 1585–1594.

Lüthi, M. and Funk, M., 2012. *Physics of Glaciers I, chapter 6: Temperatures in glaciers an ice sheets. Lecture notes ETH Zurich*.

Machguth, H., Paul, F., Hoelzle, M., and Haeberli, W., 2006. Distributed glacier mass-balance modelling as an important component of modern multi-level glacier monitoring. *Annals of Glaciology*, 43, 335–343.

Murray, T., Stuart, G.W., Miller, P.J., Woodward, J., Smith, A.M., Porter, P.R., and Jiskoot, H., 2000. Glacier surge propagation by thermal evolution at the bed. *Journal of Geophysical Research: Solid Earth (1978–2012)*, 105 (B6), 13491–13507.

Nakicenovic, N. and Swart, R., 2000. Special report on emissions scenarios. *Special Report on Emissions Scenarios, Edited by Nebojsa Nakicenovic and Robert Swart, pp. 612. ISBN 0521804930. Cambridge, UK: Cambridge University Press, July 2000.*, 1.

Nguyen, C., 1999. Subsurface sensors and applications. *In*: *SPIE proceedings series*. Denver CO.

Oerlemans, J., 2001. *Glaciers and climate change*. Lisse: A.A. Balkema.

Oerlemans, J., Giesen, R.H., and Van Den Broeke, M.R., 2009. Retreating alpine glaciers: increased melt rates due to accumulation of dust (Vadret da Morteratsch, Switzerland). *Journal of Glaciology*, 55 (192), 729–736.

Pettersson, R., 2004. Spatial variability in water content at the cold-temperate transition surface of the polythermal Storglaciären, Sweden. *Journal of Geophysical Research*, 109 (F2), F02009.

Pettersson, R., Jansson, P., and Holmlund, P., 2003. Cold surface layer thinning on Storglaciären, Sweden, observed by repeated ground penetrating radar surveys. *Journal of Geophysical Research*, 108 (F1), 1–9.

Reynolds, J.M., 2011. *An introduction to applied and environmental geophysics*. John Wiley & Sons.

Ryser, C., Lüthi, M., Blindow, N., Suckro, S., Funk, M., and Bauder, A., 2013. Cold ice in the ablation zone : Its relation to glacier hydrology and ice water content. *Journal of Geophysical Research*, 118 (October 2013), 693–705.

Sandmeier, K.J., 2013. ReflexW User Manual.

Shumsky, P.A., 1964. *Principles of structural glaciology. Translated from the Russian by D. Kraus*. New York: Dover Publications, Inc.

Stoffel, M. and Huggel, C., 2012. Effects of climate change on mass movements in mountain environments. *Progress in Physical Geography*, 36 (3), 421–439.

Suter, S. and Hoelzle, M., 2002. Cold firn in the Mont Blanc and Monte Rosa areas, European Alps: spatial distribution and statistical models. *Annals of Glaciology*, 35 (1), 9–18.

Suter, S., Laternser, M., Haeberli, W., Frauenfelder, R., and Hoelzle, M., 2001. Cold firn and ice of high-altitude glaciers in the Alps: measurements and distribution modelling. *Journal of Glaciology*, 47 (156), 85–96.

Viviroli, D., Archer, D.R., Buytaert, W., Fowler, H.J., Greenwood, G.B., Hamlet, a. F., Huang, Y., Koboltschnig, G., Litaor, M.I., López-Moreno, J.I., Lorentz, S., Schädler, B., Schreier, H., Schwaiger, K., Vuille, M., and Woods, R., 2011. Climate change and mountain water resources: overview and recommendations for research, management and policy. *Hydrology and Earth System Sciences*, 15 (2), 471–504.

Vonder Mühll, D., 1993. *Geophysikalische Untersuchungen im Permafrost des Oberengadins*.

Wagner, S., 1996. Dreidimensionale Modellierung zweier Gletscher und Deformationsanalyse von eisreichem Permafrost. *Mitteilung der Versuchsanstalt der für Wasserbau, Hydrologie und Glaziologie (VAW) der ETH Zürich*, 142, 135.

Zemp, M., Haeberli, W., Hoelzle, M., and Paul, F., 2006. Alpine glaciers to disappear within decades? *Geophysical Research Letters*, 33 (13), L13504.

Zemp, M., Hoelzle, M., and Haeberli, W., 2007. Distributed modelling of the regional climatic equilibrium line altitude of glaciers in the European Alps. *Global and Planetary Change*, 56 (1-2), 83–100.

Zhang, T., Xiao, C., Colgan, W., Qin, X., Du, W., Sun, W., Liu, Y., and Ding, M., 2013. Observed and modelled ice temperature and velocity along the main flowline of East Rongbuk Glacier, Qomolangma (Mount Everest), Himalaya. *Journal of Glaciology*, 59 (215), 438–448.

I hereby declare that the submitted thesis is the result of my own, independent work. All external sources are explicitly acknowledged in the thesis.

Nadia Signer